Evidence for, and Metabolic Consequences of, a Cardiac Mitochondrial $K_{Na}1.2$ Channel

Charles O. Smith[1], Yves T. Wang[2], Sergiy M, Nadtochiy[2], James H. Miller[2], Elizabeth A. Jonas[3], Robert, T. Dirksen[4], Keith Nehrke[4,5], Paul S. Brookes[2,4,*]

From: Departments of [1]Biochemistry, [2]Anesthesiology and Perioperative Medicine, [4]Pharmacology & Physiology, [5]Medicine, University of Rochester Medical Center, Rochester, NY 14642, USA. [3]Department of Internal Medicine, Section of Endocrinology, Yale University School of Medicine, New Haven, CT 06511, USA.

*To whom correspondence should be addressed:
Paul S. Brookes, PhD.
Department of Anesthesiology and Perioperative Medicine, Box 604,
University of Rochester Medical Center,
601 Elmwood Avenue,
Rochester, NY 14642, USA.
paul_brookes@urmc.rochester.edu
Tel… 585-273-1626

Running title: *Cardiac Mitochondrial $K_{Na}1.2$*

Abstract

Controversy surrounds the molecular identity of mitochondrial K^+ channels important for protection against cardiac ischemia-reperfusion injury. While $K_{Na}1.2$ (*Kcnt2* gene) is necessary for cardioprotection by volatile anesthetics, electrophysiologic evidence for a mitochondrial $K_{Na}1.2$ is lacking. The endogenous physiologic role of a potential mito-$K_{Na}1.2$ is also unclear. Herein, single channel patch-clamp of cardiac mitochondrial inner membranes from wild type (WT) and *Kcnt2*$^{-/-}$ mice yielded respectively 6/27 and 0/40 channels, matching the known ion-sensitivity, ion-selectivity, pharmacology and conductance properties of $K_{Na}1.2$ (WT slope conductance 138±1 pS). The K_{Na} opener bithionol uncoupled respiration in WT but not *Kcnt2*$^{-/-}$ cardiomyocytes. Furthermore, when oxidizing only fat as substrate, *Kcnt2*$^{-/-}$ cardiomyocytes and hearts were less responsive to increases in energetic demand. *Kcnt2*$^{-/-}$ mice had elevated body fat, but no baseline differences in the cardiac metabolome. These data support the existence of a cardiac mitochondrial $K_{Na}1.2$ channel with a potential metabolic regulatory role under high energetic demand.

Introduction

Numerous strategies for protection of the heart and other organs against ischemia-reperfusion (IR) injury are thought to require activation of K^+ channels in the mitochondrial inner membrane (for review see (Smith, Nehrke, & Brookes, 2017)). This includes ischemic preconditioning (IPC), volatile anesthetic preconditioning (APC), and pharmacologic cardioprotection by K^+ channel activators such as NS-11021, bithionol and diazoxide (Bentzen et al., 2007; Garlid et al., 1997; Wojtovich et al., 2016). Concurrently, several K^+ channels have been reported in mitochondria including: ATP activated (K_{ATP}) (Inoue, Nagase, Kishi, & Higuti, 1991), small conductance Ca^{2+} activated (SK) (Dolga et al., 2013; Nabbi et al., 2014), and splice variants of large conductance Ca^{2+} activated (BK) (Siemen, Loupatatzis, Borecky, Gulbins, & Lang, 1999; Singh et al., 2013). However, in only a limited number of cases has the molecular (genetic) identity of specific mitochondrial channels involved in cardioprotection been elucidated (Foster et al., 2012; Frankenreiter et al., 2017a; Singh et al., 2013; Soltysinska et al., 2014; Wojtovich et al., 2016).

Mammalian Na^+ activated K^+ (K_{Na}) channels are encoded by two genes: *Kcnt1* (Joiner et al., 1998) and *Kcnt2* (Bhattacharjee et al., 2003), which produce the $K_{Na}1.1$ (Slack/SLO2.2) and $K_{Na}1.2$ (Slick/SLO2.1) channels respectively. Both $K_{Na}1.1$ and $K_{Na}1.2$ channels play important neurologic roles in the termination of seizure progression in epilepsy (Gururaj et al., 2017; Yuki Kawasaki et al., 2017). Although $K_{Na}1.2$ is expressed in the heart (Bhattacharjee et al., 2003; Martinez-Espinosa et al., 2015), and K_{Na} channel activity has been demonstrated in the cardiac sarcolemma (Kameyama et al., 1984), the *Kcnt2*$^{-/-}$ mice have no cardiac phenotype (Martinez-Espinosa et al., 2015; Wojtovich et al., 2016). Thus relatively little is known regarding the physiologic role of $K_{Na}1.2$ channels in the heart. Previously we showed that $K_{Na}1.2$ is essential for cardiac APC, with hearts from *Kcnt2*$^{-/-}$ mice incapable of being protected against IR injury by isoflurane (Wojtovich et al., 2016). Additionally, we showed that the K_{Na} opener bithionol (BT) (Yang et al., 2006) is cardioprotective (Wojtovich et al., 2016; Yang et al., 2006) in WT mice but not *Kcnt2*$^{-/-}$ mice. Further, both BT and isoflurane activated a K^+ flux in cardiac mitochondria isolated from WT mice, but not those from *Kcnt2*$^{-/-}$ mice. These observations led us to hypothesize that $K_{Na}1.2$ is a cardiac mitochondrial K^+ channel in the heart.

While there is considerable evidence that mitochondrial K^+ channel activity can impact pathologic outcomes during IR injury (e.g., ROS generation and Ca^{2+} dysregulation (Smith et al., 2017), less is known about the endogenous physiologic role(s) of mitochondrial K^+ channels(Szabo & Zoratti, 2014). Herein, using electrophysiologic techniques (mitoplast patch-clamp) we demonstrate that $K_{Na}1.2$ is a bona-fide mitochondrial K^+ channel. Bioenergetic studies of WT and *Kcnt2*$^{-/-}$ hearts and cardiomyocytes also reveal that $K_{Na}1.2$ may have a role in the cardiac mitochondrial response to high energetic demand.

Results

Cardiac Mitochondria Contain a $K_{Na}1.2$ Channel

To investigate cardiac mitochondrial K^+ channels, we performed single channel electrophysiology studies on inside-out patches excised from Percoll™-purified isolated mitochondrial inner membranes (mitoplasts) from hearts of wild type (WT) or *Kcnt2*$^{-/-}$ mice (Figure 1A). Mitochondrial enrichment was verified by western blotting for mitochondrial

proteins, and purity was confirmed by western blotting for non-mitochondrial membrane protein contamination (Figure 1B).

Mitoplasts were adhered to glass cover slips attached to a custom 3D-printed chamber (Figure S1A). Borosilicate glass microelectrodes with resistances of 40-100 MΩ were used to form high resistance seals (2-10 GΩ) with the mitochondrial inner membrane. Excised patches were obtained in an inside-out configuration while under constant perfusion of bath solution (Figure 1A). Channel activity was consistently observed in a high proportion of patches obtained from both WT (85%) and *Kcnt2*$^{-/-}$ (76%) hearts (Figure 1C), consistent with previous reports that mitochondria contain numerous K^+ channels (Smith et al., 2017; Szewczyk, Jarmuszkiewicz, & Kunz, 2009). The bath recording solution was sequentially switched from the initial solution containing 100 µM Ca^{2+}, to 40 mM Li^+, then 40 mM Na^+, and finally 40 mM Na^+ plus 2.5 µM bithionol (BT). At each stage, channel activity was monitored across a range of holding potentials (from -100 mV to +100 mV).

In order to identify Na^+-activated K^+ channel currents, a 3 step screen was performed for each experiment, to triage recordings containing channels other than $K_{Na}1.2$ (Figure 1D-F). The first step was designed to discard recordings exhibiting channel activity in either Ca^{2+} alone or following the switch to Li^+ (8/27 WT, 22/40 *Kcnt2*$^{-/-}$ Figure 1D, gold and light-gray), as these results are indicative of K_{Ca} or Na^+-conducting channels, respectively. Next, patches exhibiting channel activity in the presence of $K_{Na}1.2$-activating levels of Na^+ (40mM) and Na^+ plus BT (2.5 µM) were considered potential $K_{Na}1.2$ candidates (12/19 WT, 8/18 *Kcnt2*$^{-/-}$ (Figure 1E blue). Recordings where channel activity in the presence of Na^+ was not observed following BT addition were discarded (3/19 WT, 1/18 *Kcnt2*$^{-/-}$ Figure 1E dark gray). Finally, single channel unitary conductance was compared to reported values for $K_{Na}1.2$ (~140 pS) (Bhattacharjee et al., 2003; Dryer, Fujii, & Martin, 1989; Kaczmarek, 2013) and those patches exhibiting the correct conductance were considered to be $K_{Na}1.2$ channels worthy of further analysis (Figure 1F red).

Figure 1G shows representative traces for channels observed in mitoplast patches from WT and *Kcnt2*$^{-/-}$ mice that exhibited different unitary conductances ranging from 40 to 650 pS, with the knockouts exhibiting an absence of activity in the conductance range expected for $K_{Na}1.2$. Quantitation of all channel conductances (Figure 1H) showed a cluster of 6 channels in WT mitoplasts that passed all screens, with an average slope conductance of 138±1 pS (Figure 1H red data points, see also Figure 2). No channels with similar conductance were observed in *Kcnt2*$^{-/-}$ mitoplasts. However, the *Kcnt2*$^{-/-}$ recordings did contain more channels (vs. WT) at a lower range of conductances (20-80 pS). Similar observations have been made for other mitochondrial K^+ channels (i.e., loss of an expected conductance in a knockout, accompanied by appearance of smaller conductances) (Frankenreiter et al., 2017b) (see Discussion). Together, the data in Figure 1 demonstrate that WT cardiac mitochondria contain a K^+ channel with the ion-selectivity, ion-sensitivity, pharmacology and conductance properties of $K_{Na}1.2$, that is absent in mitochondria from *Kcnt2*$^{-/-}$ mice.

Electrophysiologic Characterization of Mitochondrial $K_{Na}1.2$

Figure 2A shows representative examples of single channel activity for three Na^+ and BT activated conductances, recorded at a holding potential of -40 mV in WT cardiac mitoplasts. As previously reported for $K_{Na}1.2$ (Bhattacharjee et al., 2003), these channels showed rapid

flickering between open and closed states, and a unitary slope conductance of 138±1 pS (Figure 2B: peak conductance graph for all six channels). Under our buffer conditions (mM: Na^+ $[15]_{pipet}/[40]_{bath}$; Cl^- $[140]_{pipet}/[100]_{bath}$), reversal potential for channels conducting Na^+ or Cl^- is predicted to be -23 mV or -8 mV respectively. Since K^+ is the only other ion present, and the channel current crossed zero at -2 mV, this indicates that K^+ is the predominant conducting ion.

Closer examination of a representative patch with one $K_{Na}1.2$ channel (Figure 2C), revealed a higher open probability at negative potentials. Open and closed channel dwell times were calculated for 45 seconds of continuous channel recording at -40mV (Figure 2D). The frequency of channel open and closed dwell times could be fitted to the sum of multiple simple exponentials constituting 94.6% of the total area under the dwell time curve (Figures 2E and S1B). Specifically these data were fitted to a log-scale binned histogram with peaks representing two open times (A_1=20.7, τ_1 = 1.01ms, A_2=10.8, τ_2 = 2.48ms) and three closed times (A_1=29.7, τ_1 = 0.45ms, A_2=32.4, τ_2 = 1.39ms, A_3=0.88, τ_3 = 11ms). The longest closed time (τ_3) represents long periods of channel closure between bursts of activity. Additionally numerous distinct subconductances were apparent from the channel records (Figure 2F). Similar detailed single channel analyses of all experiments were not possible, due to the presence of two or more identical channels within a patch (Figures 2F and S1C). This behavior is characteristic of $K_{Na}1.1$ channels (*Kcnt1*/Slack/SLO2.2) (Kaczmarek et al., 2017; Kim & Kaczmarek, 2014) and while it has been observed in $K_{Na}1.2$ mutants (Chen et al., 2009), this is the first observation of such in WT $K_{Na}1.2$ channels in endogenous membranes.

$K_{Na}1.2$ Channel Activation Uncouples Cardiomyocyte Oxidative Phosphorylation

Having identified a cardiac mitochondrial $K_{Na}1.2$ channel, we next sought to determine its impact on mitochondrial function. Using Seahorse™ extracellular flux (XF) analysis, we measured oxygen consumption rates (OCR) of cardiomyocytes isolated from WT and *Kcnt2*$^{-/-}$ mice. Isolated cardiomyocytes from both genotypes had similar viability and rod-shaped morphology (Figure 3A). Figure 3B shows that the K_{Na} opener BT (2.5 µM) significantly stimulated OCR in oligomycin-treated cardiomyocytes from WT mice but not those from *Kcnt2*$^{-/-}$ mice (WT: 370±48 Max OCR; *Kcnt2*$^{-/-}$ 154±32 Max OCR). In the mitochondrial K^+ cycle (Garlid, 1996), K^+ entry to the organelle activates a mitochondrial K^+/H^+ exchanger, such that mitochondrial K^+ channel activity can uncouple oxidative phosphorylation. As such, the effect of BT in WT but not in *Kcnt2*$^{-/-}$ cardiomyocytes is likely due to mitochondrial uncoupling. As an additional control, the bona-fide mitochondrial uncoupler FCCP elicited similar maximal respiration rates in cardiomyocytes from both genotypes WT: 387±15 Max OCR; *Kcnt2*$^{-/-}$ 364.2±53 Max OCR), rendering it unlikely that the differential effect of BT in WT vs. *Kcnt2*$^{-/-}$ cells was due to an underlying difference in overall bioenergetic capacity. Consistent with this, western blotting for a number of mitochondrial marker enzymes (SDHA, ICDH, Cyp-D, and ETFA) revealed no differences between WT and *Kcnt2*$^{-/-}$ hearts (Figure S2), suggesting similar mitochondrial mass or content.

Loss of $K_{Na}1.2$ Mildly Impacts Cardiac Mitochondrial Ultrastructure

An important function of the mitochondrial K^+ cycle is the regulation of organelle volume (Bednarczyk et al., 2013; Checchetto, Teardo, Carraretto, Leanza, & Szabo, 2016). Thus we hypothesized that mitochondria lacking $K_{Na}1.2$ may exhibit ultrastructural changes. This

hypothesis is also supported by the finding that plasma membrane $K_{Na}1.2$ activity is sensitive to osmolarity (M. A. Tejada et al., 2014; M. A. Tejada, Hashem, Calloe, & Klaerke, 2017). Electron-microscopic analysis of hearts from WT and *Kcnt2*$^{-/-}$ mice (Figure 3C) revealed that mitochondria had similar 2-dimensional area (WT: 0.51±0.30 μm^2, *Kcnt2*$^{-/-}$: 0.53±0.32 μm^2, means±SD, N=3-4). Matrix density was also similar between genotypes (WT: 109±13, *Kcnt2*$^{-/-}$: 102±11, means±SD, N=3-4). However, the distribution of these mitochondrial parameters (Figure 3D) suggests a small shift toward increased area and density in *Kcnt2*$^{-/-}$ vs. WT (see also Figure S3). Additionally, no difference in either form-factor or aspect-ratio was observed between genotypes (Figure 3E), indicating that $K_{Na}1.2$ deficiency does not alter mitochondrial fission or fusion (Bugger et al., 2009; Picard, White, & Turnbull, 2013). Together, the data in Figure 3C-E suggest that loss of $K_{Na}1.2$ results in mild effects on cardiac mitochondrial structure without a change in overall mitochondrial mass.

K_{Na}1.2 is Required for Cardiac Respiratory Reserve Capacity when Oxidizing Fat

In an effort to further understand the bioenergetic effects of $K_{Na}1.2$ deficiency we compared metabolic substrate preferences in cardiomyocytes isolated from WT and *Kcnt2*$^{-/-}$ mice. Myocytes were incubated with either: (i) glucose alone (with etomoxir to inhibit fatty acid β-oxidation), (ii) palmitate alone (with 2-deoxyglucose to inhibit glycolysis), or (iii) glucose plus palmitate. The response to uncoupling by FCCP (500 nM) was used to determine "respiratory reserve" (RR) capacity under each substrate condition (Figures 4A-C).

Cardiomyocytes from WT and *Kcnt2*$^{-/-}$ cells exhibited a similar baseline OCR under all substrate conditions (Figure 4B open bars). In WT cells, a robust uncoupling response to FCCP was seen under all conditions, and notably the uncoupling response with palmitate alone (3.3 fold) was equal to that seen when both substrates were present (3.3 fold). However, in *Kcnt2*$^{-/-}$ cells, the uncoupling response with palmitate alone (2.4 fold) was significantly blunted compared to that seen when both substrates were present (4.3 fold) (comparison between blue and purple bars in left & right panels of Figure 4B).

The additional OCR induced over baseline by addition of FCCP is used to calculate the "respiratory reserve" (RR) capacity. Figure 4C shows that the RR of WT and *Kcnt2*$^{-/-}$ cells is similar in either the glucose alone or the glucose plus palmitate conditions (red and purple bars respectively). However, with palmitate alone (blue bars), *Kcnt2*$^{-/-}$ cells exhibit a significant RR deficit relative to WT. Notably, no such RR deficit was observed in myocytes from *Kcnt2*$^{-/-}$ mice with other substrates including: lactate, glutamine, galactose, or pyruvate (Figure S4), indicating that the *Kcnt2*$^{-/-}$ RR deficit is specific to fat oxidation.

To test the physiologic relevance of this RR deficit, the ability of perfused hearts to respond to increased metabolic demand was tested. Hearts from WT and *Kcnt2*$^{-/-}$ mice were perfused with palmitate as the sole carbon source, while stimulating workload by addition of the β-adrenergic agonist isoproterenol (100nM). Hearts from *Kcnt2*$^{-/-}$ mice showed a significantly reduced functional response to isoproterenol, relative to WT hearts (WT: 213±20 % vs. *Kcnt2*$^{-/-}$: 159±13 %, means±SEM, N=7) (Figures 4D and E). However, consistent with the isolated cardiomyocyte OCR data (Figures 4A-C), no difference in the isoproterenol-induced functional response was observed when the perfusion buffer was supplemented with glucose and palmitate (Figure 4F). Together, these data suggest that loss of $K_{Na}1.2$ results in an impaired ability to respond to increased metabolic demand when oxidizing only fat. Importantly, and

consistent with previous reports (Martinez-Espinosa et al., 2015; Wojtovich et al., 2016), no EKG differences were observed in *Kcnt2*$^{-/-}$mice (Figure S5A), suggesting that loss of K_{Na}1.2 *per se* does not impact cardiac function at baseline.

Whole Animal Metabolic Differences in Kcnt2$^{-/-}$ *Mice*

Since the heart is an important fat-burning organ, we hypothesized that the fat-specific RR deficit in *Kcnt2*$^{-/-}$ might be accompanied by metabolic perturbations at the whole animal level. No significant alterations in weight gain were observed between WT and *Kcnt2*$^{-/-}$ mice over 25 weeks (Figure 5A). Analysis of percent body fat content by differential energy X-ray absorptometry analysis (DEXA, Figure 5B) revealed a small difference in average fat content between genotypes (WT: 12.1±2.8 % vs. *Kcnt2*$^{-/-}$: 13.6±3.3 %), but nevertheless this difference was statistically significant between paired littermates (Figure 5C). In addition, while WT mice showed an expected drop in blood glucose following an overnight (15 hr.) fast, no such drop was seen in *Kcnt2*$^{-/-}$ mice (Figure 5D). This may suggest elevated gluconeogenesis in response to fasting in *Kcnt2*$^{-/-}$, which would be consistent with a shift away from fat oxidation toward an increased reliance on glucose metabolism.

Metabolomic and Expression Profiling of Kcnt2$^{-/-}$ *Hearts*

To investigate the molecular underpinnings of the fat-specific RR defect in *Kcnt2*$^{-/-}$ hearts, a predesigned qPCR array was used to examine expression of various genes that regulate metabolism (Figure 6A, Table S2). No differences were observed between hearts from WT and *Kcnt2*$^{-/-}$ mice suggesting the fat-specific RR defect is not due to a remodeling of fat metabolism at the gene level. Separately, a small but non-significant decrease in energy charge (ATP+½ADP/(ATP+ADP+AMP)) was observed in *Kcnt2*$^{-/-}$ mice (WT: 0.87±0.05 vs. *Kcnt2*$^{-/-}$: 0.77±0.03, mean±SEM, N=5-6), suggesting that energy-sensing metabolic regulators such as AMP dependent protein kinase (AMPK) may be altered. However, western blotting analyses revealed no difference in AMPK phosphorylation between WT and *Kcnt2*$^{-/-}$ hearts (Figure S2B). Furthermore, no differences were seen in the phosphorylation of the AMPK target acetyl-CoA carboxylase, or in the levels of GLUT4, PGC1-α, PPAR-α, or PPAR-γ (Figure S2C-E). Together with the data in Figure 3, these findings suggest that K_{Na}1.2 deficiency does not induce large scale remodeling of cardiac mitochondria, metabolism, or metabolic signaling. Rather, loss of K_{Na}1.2 specifically impacts cardiac fat oxidation, only under conditions of high energy demand such as uncoupling or during β-adrenergic stimulation.

Finally, to understand the effects of K_{Na}1.2 deficiency on cardiac metabolism at a systems level, an unbiased metabolomics analysis was performed. Principal component analysis (PCA) showed no significant difference in the fundamental character of metabolism between WT and *Kcnt2*$^{-/-}$hearts at baseline (Figure 6B). A volcano plot for all 501 metabolites measured revealed that only 10 were significantly altered (>1.5-fold vs. WT, $p<0.05$) (Figure 6C). Of these metabolites, notable changes were an increase in phenol-sulfate and decrease in dimethyl-sulfone, potentially indicating perturbations in aryl-sulfotransferase activity and sulfur metabolism. Dehydroascorbate was significantly lower in *Kcnt2*$^{-/-}$ hearts, potentially indicating lower oxidative load. In addition, inositol-1-phosphate was significantly elevated, and a cluster of diacylglycerol metabolites was also elevated (although no individual DAG approached significance), suggesting enhanced phospholipase C activity in *Kcnt2*$^{-/-}$ hearts. Overall, the

comparatively minor nature of metabolomic perturbations in *Kcnt2*$^{-/-}$ hearts at baseline is consistent with the notion that the impact of $K_{Na}1.2$ loss is limited to fat oxidation under conditions of high energetic demand.

Discussion

A plethora of studies has identified mitochondrial K^+ channels at the phenomenological level (reviewed in (Laskowski et al., 2016; Smith, Nehrke, & Brookes, 2017)), and several studies have linked these channels mechanistically to protection against IR injury (Ertracht, Malka, Atar, & Binah, 2014; Smith et al., 2017; Tano & Gollasch, 2014; Testai, Rapposelli, Martelli, Breschi, & Calderone, 2015). However, surprisingly few examples exist of bona-fide mitochondrial K^+ channels that are: (i) identified at the molecular (genetic) level, (ii) characterized with robust electrophysiologic studies, and (iii) linked to any specific mitochondrial channel function phenotype (Foster et al., 2012; Frankenreiter et al., 2017a; Soltysinska et al., 2014).

Using patch-clamp studies of isolated cardiac mitochondrial inner membranes (mitoplasts), we recorded a K^+ channel matching the known characteristics of $K_{Na}1.2$ channels (ion-sensitivity, ion-selectivity, pharmacology and conductance) in mitoplasts from WT mice, that was absent in those from *Kcnt2*$^{-/-}$ mice (Figure 1). Of 27 patches in WT mitoplasts, this strategy yielded 6 channels, a 22% success rate. Application of this rate to the 40 patches tested in *Kcnt2*$^{-/-}$ mitoplasts predicts 9 such patches, but we observed zero. Thus, we are confident that the molecular genetic origin of the channels herein assigned as mito-$K_{Na}1.2$, is the *Kcnt2* gene product.

Patches from WT and *Kcnt2*$^{-/-}$ recordings contained channels with a similar range of conductances. However, the distribution of these conductances between genotypes was shifted. In particular channels with unitary conductances in the range of 20-80pS were more frequently observed in the *Kcnt2*$^{-/-}$ recordings (Figure 1H). A similar observation was recently made using a cardiac-specific knockout of the mito-BK channel (Frankenreiter et al., 2017b), raising the intriguing possibility that loss of one mitochondrial K^+ channel may lead to compensatory up-regulation of other channels, to maintain a particular K^+ conductivity level. Given the importance of the mitochondrial K^+ cycle for the regulation of organelle volume (Garlid, 1996), such compensatory K^+ fluxes may also account for the relatively minuscule effect of $K_{Na}1.2$ loss on mitochondrial ultrastructure (Figure 3). Clearly, the characterization of these channels and their relationship to mitochondrial volume regulation represents an intriguing topic for future study.

In addition to straight competition or compensation between different mitochondrial K^+ channels, it is also possible that the major families of mitochondrial K^+ channels may form heterotetramers. Prior to the discovery of $K_{Na}1.2$ channels it was demonstrated that individual $K_{Na}1.1$ (*Kcnt1*) subunits could combine with $K_{Ca}1.1$ (*Kcnma1*) subunits to form functional heterotetramers of intermediate conductance and activation properties (Joiner et al., 1998). Heterotetramers of $K_{Na}1.1$ with $K_{Na}1.2$ have also been demonstrated (Chen et al., 2009). However to the best of our knowledge no studies examining $K_{Ca}1.1/K_{Na}1.2$ heterotetramers have been reported.

Although the single channel unitary slope conductance of WT mito-$K_{Na}1.2$ was 138±1 pS, our recordings revealed multiple subconductance states between 35 and 140pS (Figure 2F). These observations are in agreement with previous reports on $K_{Na}1.2$ electrophysiology

(Bhattacharjee et al., 2003; Chen et al., 2009). Examination of channel conductance including all subconductance levels revealed an average chord conductance of 74.8±6.8 pS (assuming reversal potential = 0 mV), which is in close agreement with the average slope conductance of 75 pS (Figure S1D) and indicates that smaller subconductance states predominate in the active channel current. Additionally multiple identical channels were activated within a single recording in 3 of the 6 identified mito-$K_{Na}1.2$ channel records, suggesting that $K_{Na}1.2$ channels may cluster in their endogenous membranes. Such clustering has been previously reported for $K_{Na}1.1$ channels in neuronal plasma-membranes (Kim et al., 2014).

Our recorded mito-$K_{Na}1.2$ channels were more strongly activated at negative holding potentials than positive (Figure 2C, P_{OPEN} graph). For this patch configuration (Figure 1A), negative potentials applied by the patch pipette correspond to a negative voltage on the cytosolic side of the membrane relative to the mitochondrial matrix. This is opposite the normal polarization state of the mitochondrial inner membrane (i.e., cytosolic side positive relative to the matrix). However, it should be noted that these experiments used equimolar K^+ concentrations on both sides of the patch, resulting in a reversal potential of ~0mV (Figure 2B), which may not truly reflect physiologic conditions (Hansson et al., 2010; Jung & Brierley, 1984; Klabunde, 2012; Safer & Schwartz, n.d.).

The current study represents one of only a handful of cases wherein a mitochondrial K^+ channel has been identified and characterized in mammals at the gene and protein levels (other examples include $K_{Ca}1.1$ (Frankenreiter et al., 2017b; Soltysinska et al., 2014), K_{ATP} (Foster et al., 2012), and SK3 (Stowe et al., 2013)). In addition, this is the first example of such a channel with direct ability to impact metabolism. A recent case report highlighted a patient with a $K_{Na}1.2$ mutation ($Q_{270}E$) suffering from migrating focal seizures that were non-responsive to the ketogenic diet typically used to treat such symptoms (Madaan, Jauhari, Gupta, Chakrabarty, & Gulati, 2017). Coupled with our cardiac data in *Kcnt2*$^{-/-}$ mice, this highlights potential correlations between metabolism and $K_{Na}1.2$ channels in both the heart and brain.

Notably, the metabolic phenotypes associated with loss of $K_{Na}1.2$ channels (Figures 3 and 4) were mostly observed under conditions of high energetic demand, which would correspond to classical bioenergetic "state 3", wherein the mitochondrial membrane potential is consumed to generate ATP. As such, if the *in-situ* reversal potential of mitochondrial $K_{Na}1.2$ is above zero, then channel opening could readily occur under conditions of high energetic demand when potential is lowered. In addition, the mitochondrial membrane potential is known to "flicker" *in-vivo* (O'Reilly et al., 2003), such that transient depolarization events may activate mito-$K_{Na}1.2$. Given the previously reported requirement of $K_{Na}1.2$ for cardioprotection by APC (Wojtovich et al., 2016), it is also notable that the mitochondrial membrane potential depolarizes precipitously during ischemia (Green & Kroemer, 2004; Lesnefsky, Moghaddas, Tandler, Kerner, & Hoppel, 2001). Together these observations suggest that mito-$K_{Na}1.2$ channels may be activated by acute perturbations in mitochondrial energy demand or under stress conditions such as ischemia.

In addition to acute effects on bioenergetics, the data in Figure 5 revealed that loss of $K_{Na}1.2$ resulted in altered body fat content and fasting glucose metabolism. Due to the presence of a mitochondrial K^+/H^+ exchanger (KHE), activation of a mitochondrial K^+ channel would be expected to decrease the mitochondrial ΔpH, thus uncoupling oxidative phosphorylation and stimulating OCR, as shown in Figure 3B. As such, mild mitochondrial uncoupling by mito-$K_{Na}1.2$

channel activators may represent a novel therapeutic avenue for obesity/diabetes/metabolic-syndrome. It is therefore notable that the anti-helminthic drug niclosamide, which activates K_{Na} channels (Biton et al., 2012), has long been known to uncouple mitochondria (Weinbach & Garbus, 1969), and was recently shown to confer benefits in a mouse high-fat diet model of diabetes (Tao, Zhang, Zeng, Shulman, & Jin, 2014)

Furthermore, cardiac metabolomics revealed a potential up-regulation of phospholipase C (PLC) signaling in the *Kcnt2*$^{-/-}$ heart (Figure 6C). Since K_{Na}1.2 channels are known to interact with the PLC substrate PIP_2 (M. de los A. Tejada, Jensen, & Klaerke, 2012), this raises the possibility that loss of K_{Na}1.2 results in perturbation of PIP_2/PLC signaling. An important PLC downstream target is protein kinase C epsilon (PKC_ε), which is known to play a role in development of insulin resistance in response to a high fat diet (Samuel et al., 2007). As such, in addition to mitochondrial uncoupling, mito-K_{Na}1.2 channel activators may confer metabolic benefits via a PIP_2/PLC/PKC_ε signaling axis. A deeper investigation of the relationship between mito-K_{Na}1.2 activity and metabolic regulation, is thus warranted.

Materials and Methods

Animals

Male and female mice were housed in an AAALAC-accredited pathogen-free facility with water and food available *ad libitum*. All procedures were locally approved and in accordance with the NIH *Guide for the Care and Use of Laboratory Animals* (2011 revision). All mice were on a C57BL/6J background for >6 generations and periodically backcrossed to fresh stocks. Mice were bred from *Kcnt2*$^{+/-}$ parents, and male and females were separated but littermate WT and *Kcnt2*$^{-/-}$ progeny were maintained in the same cages. Mice were genotyped by tail-clip PCR (Figure S5B), with DNA extraction by a Qiagen DNeasy™ Kit (Hilden, Germany) and genotyping by a Kapa Biosystems KAPA2G Kit (Wilmington, MA), and a BioRad thermal cycler (Carlsbad CA). Primers used were (5'→3') forward-AGGCAGCCATAGCTTTAGAGA and reverse CTCCTCATCGTGTGGTCCTA, yielding amplicons at 822 and 547 bp for WT and *Kcnt2*$^{-/-}$ respectively. Due to the same personnel handling mice and performing experiments, studies were not blinded to genotype. Patch clamp studies were performed using hearts from both male and female mice. All physiology and bioenergetics experiments were performed using hearts from male mice. Unless otherwise stated, "N" refers to data from a single mouse.

Isolated Percoll™ Purified Mitochondrial Inner Membranes (Mitoplasts)

Following anesthesia (tribromoethanol 200mg/kg ip) the heart from one 8-12 week old mouse was rapidly excised, washed and chopped in ice-cold mitochondrial isolation medium (MIM, in mM: 300 sucrose, 20 Tris, 2 EGTA, pH 7.35 at 4 °C). All steps were performed on ice. Tissue was homogenized (Tissumizer™, IKA Inc., Wilmington NC) then centrifuged at 700 x *g*, 5 min. Supernatants were saved and pellets re-homogenized and re-centrifuged. Pooled supernatants were then centrifuged at 10,000 x *g*, 10 min. The crude mitochondrial pellet was suspended in 0.2 ml MIM and layered over 1.75 ml of 30% osmotically-balanced Percoll™, in a round-bottomed microcentrifuge tube, and centrifuged at 14,000 x *g*, 1 hr. Two mitochondrial layers were apparent (Figure 1A), of which the lower (purified mitochondria) was washed twice by centrifugation. The mitochondrial pellet (~25 µl) was suspended in 0.5 ml swelling buffer (30 mM KCl, 20 mM HEPES, 1 mM EGTA, pH 7.2) for 15 min. Centrifugation (1,000 x *g*, 30 s.)

afforded a mitoplast pellet, resuspended in ~20 µl MIM for immediate use in patch-clamp studies (N=27 WT, 40 *Kcnt2*$^{-/-}$).

Patch Clamp

Mitoplasts were diluted 1:100 in patch seal buffer (in mM: 60 KCl, 80 K-gluconate, 40 LiCl, 0.025 NaCl, 0.1 $CaCl_2$ (calculated free), 20 HEPES, 1 EGTA, pH 7.2) and a 10 µl drop was placed in the center of a glass coverslip attached to a custom 3D printed micro-chamber (Figure S2). Electrodes (40-100 MΩ) (Sutter Instruments, Novato CA) were filled with pipette solution (in mM: 125 KCl, 15 K-gluconate, 15 LiCl 0.025 NaCl, 20 HEPES, 1 EGTA). Mitoplasts were identified by their round shape and presence of a "cap" structure (Figure 1A). After formation of GΩ seals, patches were excised and inside-out currents were recorded using an Axopatch 200B amplifier and Clampex10 software (Molecular Devices, Sunnyvale CA). All holding potentials reported are those applied to the patch pipette interior. The electrical connection was made using Ag/AgCl electrodes and an agar 2M KCl salt bridge at the ground electrode. (note: not all channels yielded currents at all potentials, and seal integrity was often compromised at the extremes of this range). Data was digitized and recorded at 10 kHz and filtered using an 8-pole low pass 2 kHz filter. Patches were recorded under flow (0.1 ml/min.) of: (i) Ca^{2+} free patch seal buffer with 0.076 mM sucrose for osmotic balance, (ii) as above, with LiCl replaced with 40 mM NaCl and. (iii) Further addition of 2.5 µM bithionol (BT, from stock in DMSO, final DMSO < 0.01% v/v). All buffers were filtered (0.22 µm) immediately before use. Single channel analysis was performed using Clampfit 10.0 single channel search (Molecular Devices).

Cardiomyocyte Isolation and Respiration Measurements

Mouse primary adult ventricular cardiomyocytes were isolated by collagenase perfusion as previously described (Wojtovich et al., 2016). Cells were step-wise rendered tolerant to 1.8 mM Ca^{2+}, and the final pellet suspended in 1 ml MEM (GIBCO cat # 11095-080, supplemented with 1.8 mM, $CaCl_2$ 2.5% FBS and pen/strep). Cell viability and yield were determined using Trypan blue and a hemocytometer. Only preparations with >85% viable rod-shaped cells were used for experiments. Cells were seeded at 2000/well on Seahorse™ XF96 V3-PS plates (Agilent, Billerica MA) and equilibrated for 1 hr. MEM was replaced with unbuffered DMEM (pH 7.4) containing various carbon sources (in mM 5 glucose, 0.1 palmitate, 4 glutamine, 5 galactose, 5 lactate, 1 pyruvate) and either 10 mM 2-deoxyglucose or 20 µM etomixir as detailed in results. All conditions with palmitate had 0.1 mM L-carnitine. Oxygen consumption rates (OCR) were measured using an XF96 extracellular flux analyzer.

Ex-vivo Heart Perfusion

Mouse hearts were perfused in constant flow (4ml/min) Langendorff mode as previously described (Wojtovich et al., 2016). Krebs-Henseleit buffer (KH, in mM: 118 NaCl, 4.7 KCl, 25 $NaHCO_3$, 1.2 $MgSO_4$, 1.2 KH_2PO_4, and 2.5 $CaCl_2$, gassed with 95/5 O_2/CO_2, 37 °C) was supplemented with either 5 mM glucose, or 0.1 mM BSA-conjugated palmitate. Left ventricular pressure was measured via a water-filled transducer-linked left ventricular balloon. Left ventricular and coronary root pressures were monitored and digitally recorded at 1 kHz

(DATAQ, Akron OH). After equilibration hearts were treated with isoproterenol (100 nM final) for 5 min.

Electron Microscopy

Hearts were fixed in 4 % paraformldehyde + 2.5 % glutaraldehyde in Millonig's phosphate buffer (0.2 M NaH_2PO_4/Na_2HPO_4, 0.5 % NaCl, pH 7.4). 1 mm cubes were processed and digitally photographed on a Hitachi 7650 electron microscope. Analysis of images was performed using NIH ImageJ software. Mitochondrial areas and density were placed in to 11 or 13 bins respectively and the resulting histograms were fitted to a single Gaussian. Form-factor was calculated as $1/((4\pi.\text{area})/(\text{perimeter}^2))$ and aspect-ratio was calculated as (major axis/minor axis).

Metabolomics

WT and *Kcnt2*$^{-/-}$ hearts (N=7 per group) were perfused as above in KH buffer supplemented with glucose plus palmitate for 20 min., then freeze-clamped with Wollenberger tongs in liquid N_2 and ground to powder. Samples representing ~50% of each heart (50 mg) were shipped to Metabolon Inc. (Research Triangle Park, NC) on dry ice, extracted by standard procedures, and analyzed by LC-MS/MS and GC-MS/MS (Metabolon "Global Metabolomics" solution) to measure the relative steady-state abundance of metabolites.

Data for each run were median-normalized. Overall, 527 metabolites were identified, of which 26 (4.9%) were removed due to insufficient replicates, yielding 7014 theoretical individual data points (501 x N=7 x 2 groups). A further 229 outliers (>1 standard deviation from the mean) were removed, representing 3.3 % of the data. Missing values were imputed as weighted medians (Aittokallio, 2010). Metabolomic data were analyzed using free Metaboanalyst software (Xia & Wishart, 2016). In a separate series of experiments, WT and *Kcnt2*$^{-/-}$ hearts were perfused in KH buffer supplemented with fat as the only carbon source, and adenine nucleotide levels (ATP, ADP, AMP) were measured as previously described (Nadtochiy et al., 2015). Energy charge was calculated as (ATP+½ADP/(ATP+ADP+AMP).

Immunoblotting

Sample protein was determined by the Folin-Phenol (Lowry) assay. Non-mitochondrial samples were diluted 2x in Laemmli sample loading buffer (SLB) and incubated at 95 °C for 1 min., while mitochondrial samples were diluted in SLB containing 5x the standard concentration of SDS and incubated at 25 °C for 30 min. Samples were separated by SDS-PAGE (10% gels) and transferred to nitrocellulose, followed by probing with antibodies as recommended by manufacturer protocols (see Table S2). Detection employed HRP-linked secondary antibodies with enhanced chemiluimnescence (GE Biosciences). Developed ECL film images were quantified by densitometry using NIH ImageJ software (N=3-4 mice per genotype).

Body Composition, Fasting Glucose Response, and Electrocardiogram

84 day old (12 week) WT and littermate *Kcnt2*$^{-/-}$ male mice were anesthetized as described above, and body fat content measured using dual energy X-ray absorptometry (DEXA) scanning (Lunar PIXImus densitometer, GE, Fitchburg WI). Blood glucose was measured using a True2Go™ glucose meter with TrueTest™ glucose strips (Trividia Health, Fort Lauderdale

FL). Mice were fasted overnight in cleaned cages with access to water and cotton bedding. Alternatively, after anesthesia mice electrocardiograms were recorded using a three electrode EKG amplifier (Harvard Apparatus, Cambridge MA). EKGs were averaged for each animal from ten different segments of the trace, each containing R_1-S_1-T_1-P_2-Q_2-R_2 waves.

qPCR analysis

mRNA was extracted from heart homogenates with acid phenol/TRIzol according to the Direct-zol RNA MiniPrep Kit R2050 (Zymo Research, Irvine CA) as described (Toledo-Arana et al., 2009). cDNAs were prepared using an iScript kit (170-8891, BioRad). qPCR analysis was performed using a BioRad PrimePCR™ "Regulation of lipid metabolism-PPAR" M96 Predesigned 96-well panel for use with SYBR® Green (Cat # 10031585).

Replicates & Statistics

Numbers of individual replicates for experiments are listed in each figure legend. For samples comparing WT and *Kcnt2*$^{-/-}$, one "N" equals one animal (i.e., biological replicates). Statistical differences between WT and *Kcnt2*$^{-/-}$ were determined using two-way ANOVA with a Bonferroni correction for multiple testing, followed by post-hoc paired or non-paired *t*-tests ($p<0.05$ cut-off).

Funding

This work was funded by grants from the National Institutes of Health: R01-GM087483 (to PSB and KN), R01-HL071158 (to PSB) and R01-AR-059646 (to RTD).

Disclosures

None

Acknowledgments.

We thank Christopher Lingle (Washington University, St Louis MO) for providing founders for the *Kcnt2*$^{-/-}$ mice, and Kathleen Kinally (New York University, Emeritus) for technical support in performing mitochondrial patch clamp experiments. We also thank Dana Godfrey (URMC musculoskeletal center) for support with DEXA analyses, and Karen Bentley (URMC electron microscopy core).

References

Aittokallio, T. (2010). Dealing with missing values in large-scale studies: microarray data imputation and beyond. *Briefings in Bioinformatics*, *11*(2), 253–264. https://doi.org/10.1093/bib/bbp059

Bednarczyk, P., Wieckowski, M. R., Broszkiewicz, M., Skowronek, K., Siemen, D., & Szewczyk, A. (2013). Putative Structural and Functional Coupling of the Mitochondrial BKCa Channel to the Respiratory Chain. *PLoS ONE*, *8*(6). https://doi.org/10.1371/journal.pone.0068125

Bentzen, B. H., Nardi, A., Calloe, K., Madsen, L. S., Olesen, S.-P., & Grunnet, M. (2007). The Small Molecule NS11021 Is a Potent and Specific Activator of Ca2+-Activated Big-Conductance K+ Channels. *Molecular Pharmacology*, *72*(4), 1033–1044.

519 https://doi.org/10.1124/mol.107.038331
520 Bhattacharjee, A., Joiner, W. J., Wu, M., Yang, Y., Sigworth, F. J., & Kaczmarek, L. K. (2003). Slick
521 (Slo2.1), a rapidly-gating sodium-activated potassium channel inhibited by ATP. *The*
522 *Journal of Neuroscience : The Official Journal of the Society for Neuroscience*, *23*(37),
523 11681–11691. https://doi.org/23/37/11681 [pii]
524 Biton, B., Sethuramanujam, S., Picchione, K. E., Bhattacharjee, A., Khessibi, N., Chesney, F., …
525 Avenet, P. (2012). The antipsychotic drug loxapine is an opener of the sodium-activated
526 potassium channel slack (Slo2.2)., *340*(3). https://doi.org/10.1124/jpet.111.184622
527 Bugger, H., Dong, C., Riehle, C., Soto, J., Theobald, H. A., Hu, X., … Abel, E. D. (2009). Tissue-
528 specific remodeling of the mitochondrial proteome in type 1 diabetic akita mice. *Diabetes*,
529 *58*(9), 1986–1997. https://doi.org/10.2337/db09-0259
530 Checchetto, V., Teardo, E., Carraretto, L., Leanza, L., & Szabo, I. (2016). Physiology of
531 intracellular potassium channels: A unifying role as mediators of counterion fluxes?,
532 *1857*(8). https://doi.org/10.1016/j.bbabio.2016.03.011
533 Chen, H., Kronengold, J., Yan, Y., Gazula, V.-R. V.-R., Brown, M. R., Ma, L., … Kaczmarek, L. K.
534 (2009). The N-terminal domain of Slack determines the formation and trafficking of
535 Slick/Slack heteromeric sodium-activated potassium channels. *The Journal of*
536 *Neuroscience : The Official Journal of the Society for Neuroscience*, *29*(17), 5654–5665.
537 https://doi.org/10.1523/JNEUROSCI.5978-08.2009
538 Dolga, A. M., Netter, M. F., Perocchi, F., Doti, N., Meissner, L., Tobaben, S., … Culmsee, C.
539 (2013). Mitochondrial small conductance SK2 channels prevent glutamate-induced
540 oxytosis and mitochondrial dysfunction. *The Journal of Biological Chemistry*, *288*(15),
541 10792–804. https://doi.org/10.1074/jbc.M113.453522
542 Dryer, S. E., Fujii, J. T., & Martin, A. R. (1989). A Na+-activated K+ current in cultured brain stem
543 neurones from chicks. *The Journal of Physiology*, *410*, 283–96. Retrieved from
544 http://www.ncbi.nlm.nih.gov/pubmed/2795480
545 Ertracht, O., Malka, A., Atar, S., & Binah, O. (2014). The mitochondria as a target for
546 cardioprotection in acute myocardial ischemia. *Pharmacology & Therapeutics*, *142*(1), 33–
547 40. https://doi.org/10.1016/j.pharmthera.2013.11.003
548 Foster, D. B., Ho, A. S., Rucker, J., Garlid, A. O., Chen, L., Sidor, A., … O'Rourke, B. (2012).
549 Mitochondrial ROMK channel is a molecular component of mitoK(ATP). *Circulation*
550 *Research*, *111*(4), 446–54. https://doi.org/10.1161/CIRCRESAHA.112.266445
551 Frankenreiter, S., Bednarczyk, P., Kniess, A., Bork, N., Straubinger, J., Koprowski, P., … Lukowski,
552 R. (2017a). cGMP-Elevating Compounds and Ischemic Conditioning Provide
553 Cardioprotection Against Ischemia and Reperfusion Injury via Cardiomyocyte-Specific BK
554 Channels. *Circulation*, CIRCULATIONAHA.117.028723.
555 https://doi.org/10.1161/CIRCULATIONAHA.117.028723
556 Frankenreiter, S., Bednarczyk, P., Kniess, A., Bork, N., Straubinger, J., Koprowski, P., … Lukowski,
557 R. (2017b). cGMP-Elevating Compounds and Ischemic Conditioning Provide
558 Cardioprotection Against Ischemia and Reperfusion Injury via Cardiomyocyte-Specific BK
559 Channels. *Circulation*, CIRCULATIONAHA.117.028723.
560 https://doi.org/10.1161/CIRCULATIONAHA.117.028723
561 Garlid, K. D. (1996). Cation transport in mitochondria--the potassium cycle. *Biochimica et*
562 *Biophysica Acta*, *1275*(1–2), 123–6. Retrieved from

563 http://www.ncbi.nlm.nih.gov/pubmed/8688444
564 Garlid, K. D., Paucek, P., Yarov-Yarovoy, V., Murray, H. N., Darbenzio, R. B., D'Alonzo, A. J., …
565 Grover, G. J. (1997). Cardioprotective effect of diazoxide and its interaction with
566 mitochondrial ATP-sensitive K+ channels. Possible mechanism of cardioprotection.
567 *Circulation Research*, *81*(6), 1072–82. Retrieved from
568 http://www.ncbi.nlm.nih.gov/pubmed/9400389
569 Green, D. R., & Kroemer, G. (2004). The pathophysiology of mitochondrial cell death. *Science*
570 *(New York, N.Y.)*, *305*(5684), 626–9. https://doi.org/10.1126/science.1099320
571 Gururaj, S., Palmer, E. E., Sheehan, G. D., Kandula, T., Macintosh, R., Ying, K., … Bhattacharjee,
572 A. (2017). A De Novo Mutation in the Sodium-Activated Potassium Channel KCNT2 Alters
573 Ion Selectivity and Causes Epileptic Encephalopathy. *Cell Reports*, *21*(4), 926–933.
574 Retrieved from http://linkinghub.elsevier.com/retrieve/pii/S2211124717314080
575 Hansson, M. J., Morota, S., Teilum, M., Mattiasson, G., Uchino, H., & Elmér, E. (2010). Increased
576 potassium conductance of brain mitochondria induces resistance to permeability
577 transition by enhancing matrix volume. *Journal of Biological Chemistry*, *285*(1), 741–750.
578 https://doi.org/10.1074/jbc.M109.017731
579 Inoue, I., Nagase, H., Kishi, K., & Higuti, T. (1991). ATP-sensitive K+ channel in the mitochondrial
580 inner membrane. *Nature*, *352*(6332), 244–247. https://doi.org/10.1038/352244a0
581 Joiner, W. J., Tang, M. D., Wang, L.-Y. Y., Dworetzky, S. I., Boissard, C. G., Gan, L., … Kaczmarek,
582 L. K. (1998). Formation of intermediate-conductance calcium-activated potassium channels
583 by interaction of Slack and Slo subunits. *Nature Neuroscience*, *1*(6), 462–469.
584 https://doi.org/10.1038/2176
585 Jung, D. W., & Brierley, G. P. (1984). THE JOURNAL OF BIOLOGICAL CHEMISTRY The Permeability
586 of Uncoupled Heart Mitochondria to Potassium Ion*, *259*(11), 6904–6911. Retrieved from
587 http://www.jbc.org/content/259/11/6904.full.pdf
588 Kaczmarek, L. K. (2013). Slack, Slick and Sodium-Activated Potassium Channels. *ISRN*
589 *Neuroscience*, *2013*(2013), 1–14. https://doi.org/10.1155/2013/354262
590 Kaczmarek, L. K., Aldrich, R. W., Chandy, K. G., Grissmer, S., Wei, A. D., & Wulff, H. (2017).
591 International Union of Basic and Clinical Pharmacology . C . Nomenclature and Properties
592 of Calcium-Activated and Sodium-Activated Potassium Channels. *Pharmacological Reviews*,
593 *69*(1), 1–11. https://doi.org/10.1124/pr.116.012864
594 Kameyama, M., Kakei, M., Sato, R., Shibasaki, T., Matsuda, H., & Irisawa, H. (1984). Intracellular
595 Na+ activates a K+ channel in mammalian cardiac cells. *Nature*, *309*(5966), 354–356.
596 https://doi.org/10.1038/309354a0
597 Kim, G. E., & Kaczmarek, L. K. (2014). Emerging role of the KCNT1 Slack channel in intellectual
598 disability. *Frontiers in Cellular Neuroscience*, *8*, 209.
599 https://doi.org/10.3389/fncel.2014.00209
600 Kim, G. E., Kronengold, J., Barcia, G., Quraishi, I. H., Martin, H. C., Blair, E., … Kaczmarek, L. K.
601 (2014). Human Slack Potassium Channel Mutations Increase Positive Cooperativity
602 between Individual Channels. *Cell Reports*, *9*(5), 1661–1672.
603 https://doi.org/10.1016/j.celrep.2014.11.015
604 Klabunde, R. E. (2012). *Cardiovascular physiology concepts*. Lippincott Williams &
605 Wilkins/Wolters Kluwer. Retrieved from http://www.cvphysiology.com/textbook
606 Laskowski, M., Augustynek, B., Kulawiak, B., Koprowski, P., Bednarczyk, P., Jarmuszkiewicz, W.,

& Szewczyk, A. (2016). What do we not know about mitochondrial potassium channels? *Biochimica et Biophysica Acta (BBA) - Bioenergetics*, *1857*(8), 1247–1257. https://doi.org/10.1016/j.bbabio.2016.03.007

Lesnefsky, E. J., Moghaddas, S., Tandler, B., Kerner, J., & Hoppel, C. L. (2001). Mitochondrial Dysfunction in Cardiac Disease: Ischemia–Reperfusion, Aging, and Heart Failure. *Journal of Molecular and Cellular Cardiology*, *33*(6), 1065–1089. https://doi.org/10.1006/jmcc.2001.1378

Madaan, P., Jauhari, P., Gupta, A., Chakrabarty, B., & Gulati, S. (2017). A quinidine non responsive novel KCNT1 mutation in an Indian infant with epilepsy of infancy with migrating focal seizures. *Brain and Development*. https://doi.org/10.1016/j.braindev.2017.09.008

Martinez-Espinosa, P. L., Wu, J., Yang, C., Gonzalez-Perez, V., Zhou, H., Liang, H., … Lingle, C. J. (2015). Knockout of Slo2.2 enhances itch, abolishes KNa current, and increases action potential firing frequency in DRG neurons. *eLife*, *4*(NOVEMBER2015), 1–27. https://doi.org/10.7554/eLife.10013

Nabbi, R., Gadicherla, A. K., Kersten, J. R., Stowe, D. F., Lazar, J., & Riess, M. L. (2014). Genetically determined mitochondrial preservation and cardioprotection against myocardial ischemia-reperfusion injury in a consomic rat model. *Physiological Genomics*, *46*(5), 169–76. https://doi.org/10.1152/physiolgenomics.00118.2013

Nadtochiy, S. M., Urciuoli, W., Zhang, J., Schafer, X., Munger, J., & Brookes, P. S. (2015). Metabolomic profiling of the heart during acute ischemic preconditioning reveals a role for SIRT1 in rapid cardioprotective metabolic adaptation. *Journal of Molecular and Cellular Cardiology*, *88*, 64–72. https://doi.org/10.1016/j.yjmcc.2015.09.008

O'Reilly, C. M., Fogarty, K. E., Drummond, R. M., Tuft, R. A., Walsh, J. V, & Jr. (2003). Quantitative analysis of spontaneous mitochondrial depolarizations. *Biophysical Journal*, *85*(5), 3350–7. https://doi.org/10.1016/S0006-3495(03)74754-7

Picard, M., White, K., & Turnbull, D. M. (2013). Mitochondrial morphology, topology, and membrane interactions in skeletal muscle: a quantitative three-dimensional electron microscopy study. *Journal of Applied Physiology*, *114*(2), 161–171. https://doi.org/10.1152/japplphysiol.01096.2012

Safer, B., & Schwartz, A. A. (n.d.). Active Transport of Potassium Ion in Heart Mitochondria. Retrieved from https://pdfs.semanticscholar.org/e354/e8ec9ff900e15b5c6395ea2cd21b4ac5bee6.pdf

Samuel, V. T., Liu, Z.-X., Wang, A., Beddow, S. A., Geisler, J. G., Kahn, M., … Shulman, G. I. (2007). Inhibition of protein kinase Cepsilon prevents hepatic insulin resistance in nonalcoholic fatty liver disease. *The Journal of Clinical Investigation*, *117*(3), 739–45. https://doi.org/10.1172/JCI30400

Siemen, D., Loupatatzis, C., Borecky, J., Gulbins, E., & Lang, F. (1999). Ca2+-activated K channel of the BK-type in the inner mitochondrial membrane of a human glioma cell line. *Biochemical and Biophysical Research Communications*, *257*(2), 549–54. https://doi.org/10.1006/bbrc.1999.0496

Singh, H., Lu, R., Bopassa, J. C., Meredith, A. L., Stefani, E., & Toro, L. (2013). MitoBK(Ca) is encoded by the Kcnma1 gene, and a splicing sequence defines its mitochondrial location. *Proceedings of the National Academy of Sciences of the United States of America*, *110*(26),

651 10836–41. https://doi.org/10.1073/pnas.1302028110
652 Smith, C. O., Nehrke, K., & Brookes, P. S. (2017). The Slo(w) path to identifying the
653 mitochondrial channels responsible for ischemic protection. *Biochemical Journal*, *474*(12),
654 2067–2094. https://doi.org/10.1042/BCJ20160623
655 Soltysinska, E., Bentzen, B. H., Barthmes, M., Hattel, H., Thrush, A. B., Harper, M.-E. E., …
656 Lukowski, R. (2014). KCNMA1 encoded cardiac BK channels afford protection against
657 ischemia-reperfusion injury. *PLoS ONE*, *9*(7), e103402.
658 https://doi.org/10.1371/journal.pone.0103402
659 Stowe, D. F., Gadicherla, A. K., Zhou, Y., Aldakkak, M., Cheng, Q., Kwok, W.-M., … Camara, A. K.
660 S. S. (2013). Protection against cardiac injury by small Ca(2+)-sensitive K(+) channels
661 identified in guinea pig cardiac inner mitochondrial membrane. *Biochimica et Biophysica*
662 *Acta*, *1828*(2), 427–42. https://doi.org/10.1016/j.bbamem.2012.08.031
663 Szabo, I., & Zoratti, M. (2014). Mitochondrial channels: ion fluxes and more. *Physiological*
664 *Reviews*, *94*(2), 519–608. https://doi.org/10.1152/physrev.00021.2013
665 Szewczyk, A., Jarmuszkiewicz, W., & Kunz, W. S. (2009). Mitochondrial potassium channels.
666 *IUBMB Life*, *61*(2), 134–143. https://doi.org/10.1002/iub.155
667 Tano, J.-Y. J.-Y., & Gollasch, M. (2014). Hypoxia and ischemia-reperfusion: a BiK contribution?
668 *AJP: Heart and Circulatory Physiology*, *307*(6), H811–H817.
669 https://doi.org/10.1152/ajpheart.00319.2014
670 Tao, H., Zhang, Y., Zeng, X., Shulman, G. I., & Jin, S. (2014). Niclosamide ethanolamine–induced
671 mild mitochondrial uncoupling improves diabetic symptoms in mice. *Nature Medicine*,
672 *20*(11), 1263–1269. https://doi.org/10.1038/nm.3699
673 Tejada, M. A., Hashem, N., Calloe, K., & Klaerke, D. A. (2017). Heteromeric Slick/Slack K+
674 channels show graded sensitivity to cell volume changes. *PloS One*, *12*(2), e0169914.
675 https://doi.org/10.1371/journal.pone.0169914
676 Tejada, M. A., Stople, K., Hammami Bomholtz, S., Meinild, A.-K., Poulsen, A. N., & Klaerke, D. A.
677 (2014). Cell volume changes regulate slick (Slo2.1), but not slack (Slo2.2) K+ channels. *PloS*
678 *One*, *9*(10), e110833. https://doi.org/10.1371/journal.pone.0110833
679 Tejada, M. de los A., Jensen, L. J., & Klaerke, D. A. (2012). PIP2 modulation of Slick and Slack K+
680 channels. *Biochemical and Biophysical Research Communications*, *424*(2), 208–213.
681 https://doi.org/10.1016/j.bbrc.2012.06.038
682 Testai, L., Rapposelli, S., Martelli, A., Breschi, M. C., & Calderone, V. (2015). Mitochondrial
683 Potassium Channels as Pharmacological Target for Cardioprotective Drugs. *Medicinal*
684 *Research Reviews*, *35*(3), 520–553. https://doi.org/10.1002/med.21332
685 Toledo-Arana, A., Dussurget, O., Nikitas, G., Sesto, N., Guet-Revillet, H., Balestrino, D., …
686 Cossart, P. (2009). The Listeria transcriptional landscape from saprophytism to virulence.
687 *Nature*, *459*(7249), 950–956. https://doi.org/10.1038/nature08080
688 Weinbach, E. C., & Garbus, J. (1969). Mechanism of action of reagents that uncouple oxidative
689 phosphorylation. *Nature*, *221*(5185), 1016–8. Retrieved from
690 http://www.ncbi.nlm.nih.gov/pubmed/4180173
691 Wojtovich, A. P., Smith, C. O., Urciuoli, W. R., Wang, Y. T., Xia, X.-M., Brookes, P. S., & Nehrke, K.
692 (2016). Cardiac Slo2.1 Is Required for Volatile Anesthetic Stimulation of K+ Transport and
693 Anesthetic Preconditioning. *Anesthesiology*, *124*(5), 1065–76.
694 https://doi.org/10.1097/ALN.0000000000001046

695 Xia, J., & Wishart, D. S. (2016). Using MetaboAnalyst 3.0 for Comprehensive Metabolomics Data
696 Analysis. In *Current Protocols in Bioinformatics* (Vol. 55, p. 14.10.1-14.10.91). Hoboken, NJ,
697 USA: John Wiley & Sons, Inc. https://doi.org/10.1002/cpbi.11
698 Yang, B., Gribkoff, V. K., Pan, J., Damagnez, V., Dworetzky, S. I., Boissard, C. G., … Kaczmarek, L.
699 K. (2006). Pharmacological activation and inhibition of Slack (Slo2.2) channels.
700 *Neuropharmacology*, *51*(4), 896–906. https://doi.org/10.1016/j.neuropharm.2006.06.003
701 Yuki Kawasaki, M., , Ichiro Kuki, M., , Eiji Ehara, M., , Yosuke Murakami, M., , Shin Okazaki, M., ,
702 Hisashi Kawawaki, M., … , and Naomichi Matsumoto, MD, P. (2017). Three Cases of KCNT1
703 Mutations: Malignant Migrating Partial Seizures in Infancy with Massive Systemic to
704 Pulmonary Collateral Arteries. *The Journal of Pediatrics*.
705 https://doi.org/10.1016/J.JPEDS.2017.08.057
706
707

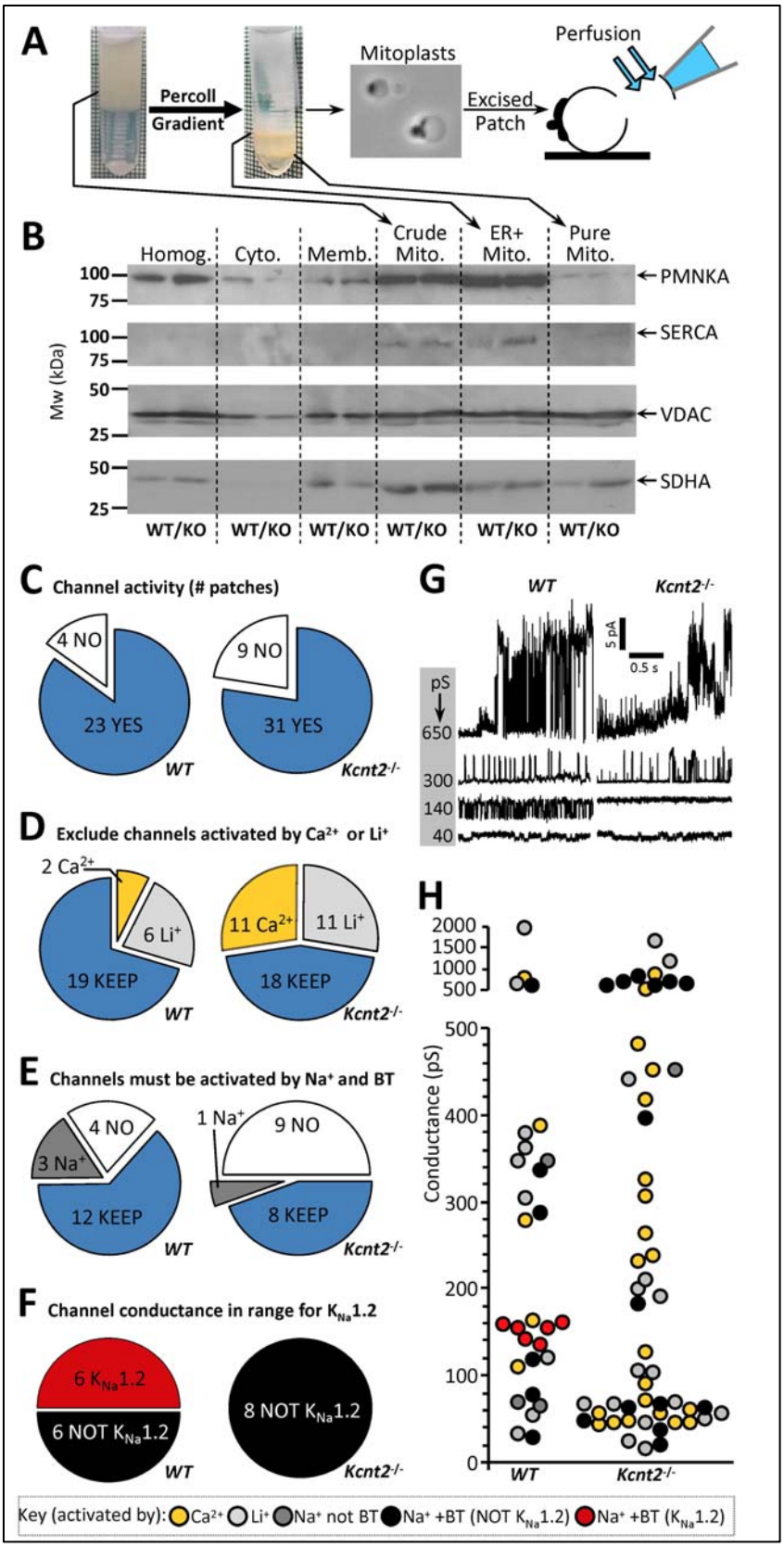

Figure 1: Mitochondria Contain a $K_{Na}1.2$ Channel. (A) Schematic depicting mitochondrial purification, mitoplast preparation, and excised patch configuration. **(B)** Western blot of proteins from different cellular fractions during mitochondrial purification. (Homog: homogenate, Cyto: cytosol, Memb: crude membrane, Crude Mito: mitochondrial enriched fraction, ER+Mito: upper band following Percoll™, Pure Mito: lower band following Percoll™). PMNKA: plasma membrane Na^+/K^+-ATPase, SERCA: sarco-endoplasmic reticulum Ca^{2+}-ATPase, VDAC: mitochondrial outer membrane voltage dependent anion channel, SDHA: mitochondrial inner membrane succinate dehydrogenase subunit A. **(C)** Patches from WT (left) and *Kcnt2*$^{-/-}$ (right) mitoplasts, sorted by channels observed (blue) or no channels observed (white). **(D)** Exclusion of Ca^{2+}-activated (gold) or Li^+-activated (light gray) channels. **(E)** Selection of channels activated by Na^+ and bithionol (BT), with exclusion of channels activated by Na^+ alone and blocked by BT (dark gray). For panels C-E, channels carried over to the subsequent screening step are shown in blue. **(F)** Selection of channels with peak conductance matching $K_{Na}1.2$ (red). **(G)** Example traces of channels observed in WT and *Kcnt2*$^{-/-}$ preparations with a variety of peak conductances (pS, shown in gray inset). **(H)** Peak conductances of channels observed from all traces. Note that some patches yielded traces with more than one channel, such that number of points in panel H is greater than WT 23, KO 31 (number of patches) in panel C. Color key for panels D,E,F,H shown at base of Figure.

759

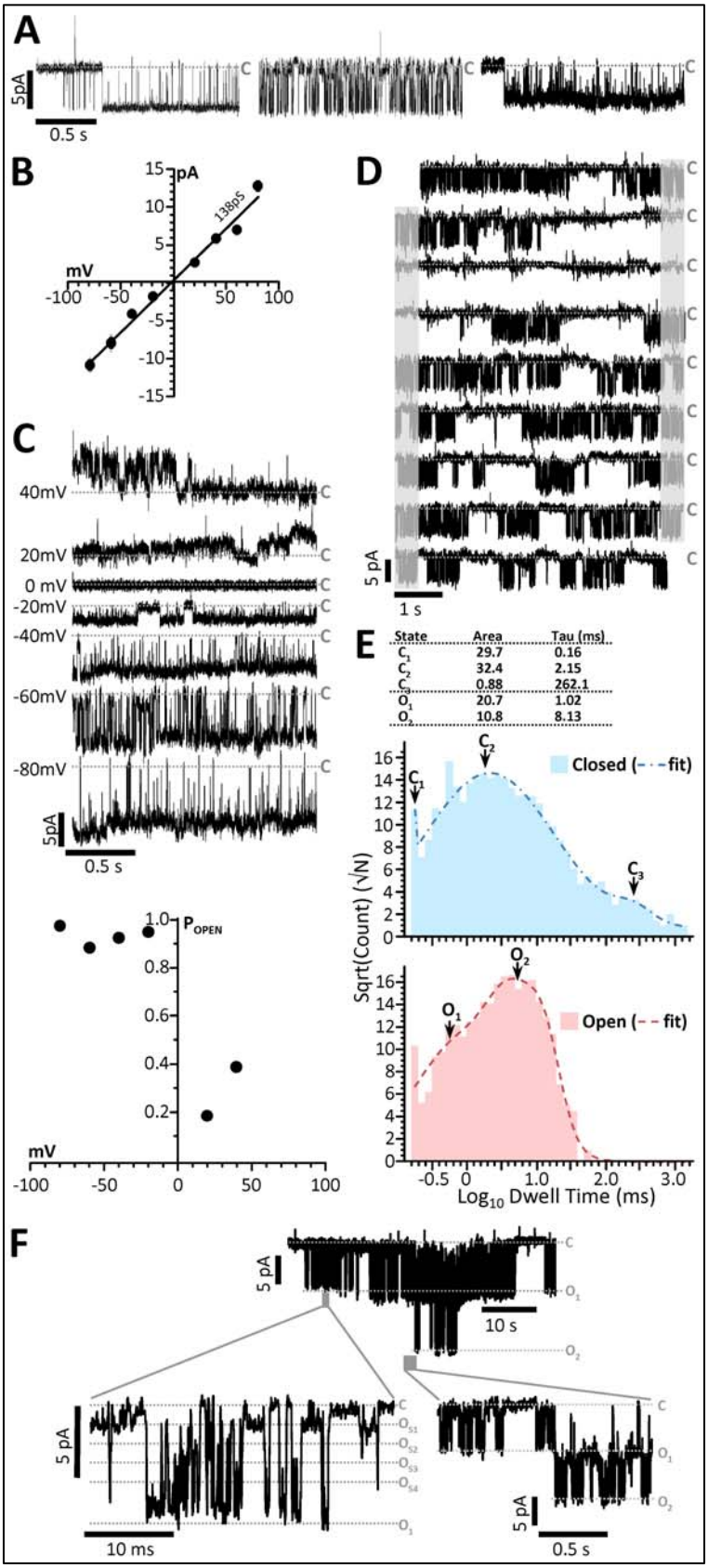

Figure 2: Single Channel Characteristics of Mitochondrial $K_{Na}1.2$. (A) Example of 2 s recordings from three $K_{Na}1.2$ channels observed in WT mitoplasts (i.e., red points in Figure 1H) at -40 mV holding potential. Current scale bar indicated at left. Closed states are indicated by gray dashed line labeled "C". **(B)** Channel current vs. voltage plot of peak unitary conductances of $K_{Na}1.2$ channels from WT mitoplast recordings. Slope conductance of 138±1 pS. **(C)** Traces from a single $K_{Na}1.2$ channel, at holding potentials of 40mV to -80mV (upper panel). Channel open probability plot (lower panel) from this channel. **(D)** 45 s continuous trace of a single channel. Gray areas indicate portions of each trace (right) which are repeated (left) on the next line. Closed states are indicated by gray dashed line labeled "C". **(E)** Log binned channel open (salmon) and closed (sky blue) dwell-time peaks. Table insert above shows calculated Area and time constant (τ) values. **(F)** Representative trace of a recording with multiple $K_{Na}1.2$ channels on a compressed time scale (upper) and expanded view of subconductances within the channel peak conductance (left) or multiple channels (right).

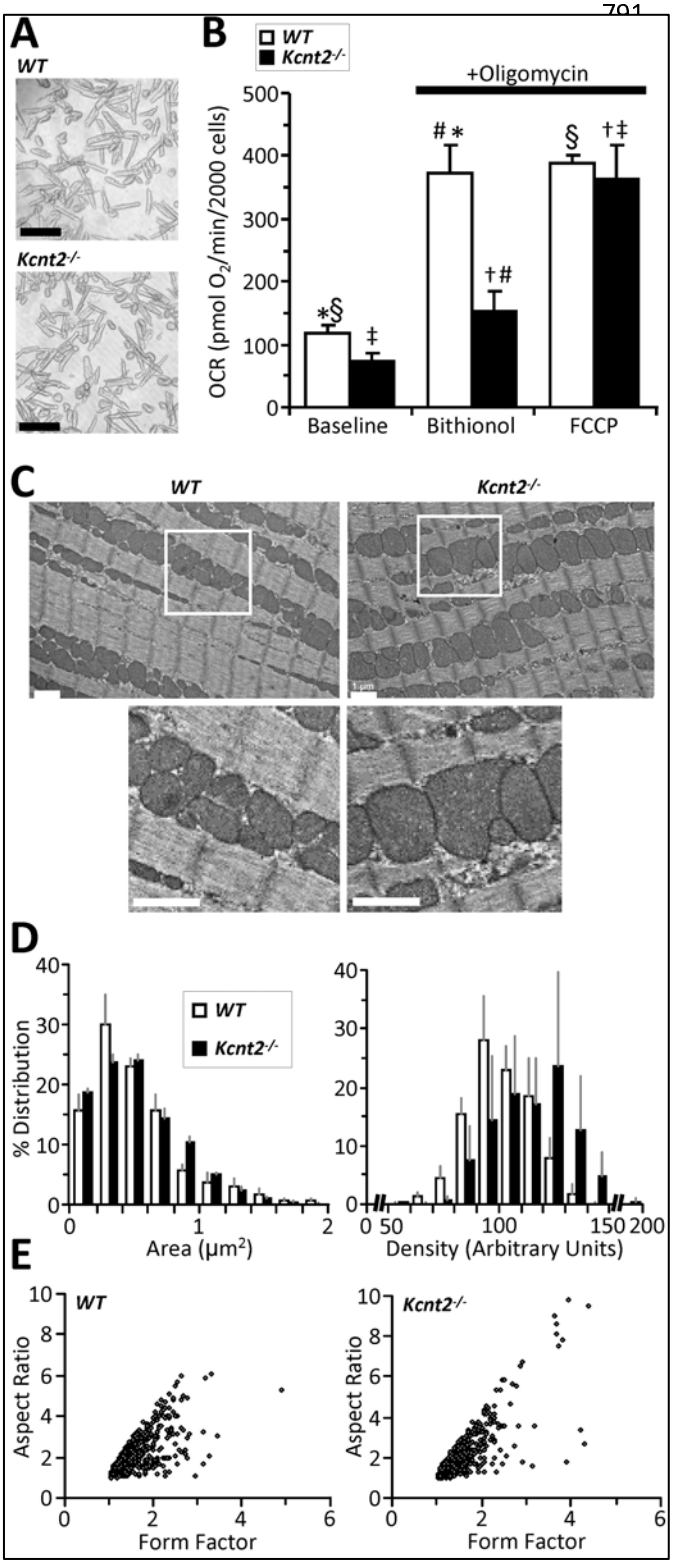

Figure 3: *Kcnt2*$^{-/-}$, Cardiomyocyte Bioenergetics and Mitochondrial Structure. (A) Representative images of isolated cardiomyoctes from WT and *Kcnt2*$^{-/-}$ hearts. Black scale bar is 100 µm. **(B)** Oxygen consumption rate (OCR) of isolated cardiomyocytes measured in XF96 Seahorse Analyzer, with addition of oligomycin (1µg/ml) and either 2.5 µM bithionol (K_{Na} opener) or 500 nM FCCP (mitochondrial uncoupler). Statistics were measured using 2-way ANOVA with Bonferroni correction and post-hoc *t*-test. Bars with the same symbol are significantly different from each other ($p<0.05$). Data are means±SEM, N=4-5. **(C)** Representative transmission electron microscope images from fixed heart slices. Lower panels show inset boxes at higher magnification. Both white scale bars = 1 µm. **(D)** Binned histogram of mitochondrial area or mitochondrial density, obtained from analysis of mitochondria using ImageJ software. Data are means±SEM for each bin, N=3-4. **(E)** Form-factor/aspect-ratio scatter plot. Values in panels D and E were obtained from N=1054/789 mitochondria, from 17/14 fields of view, from 4/3 hearts, of WT/*Kcnt2*$^{-/-}$.

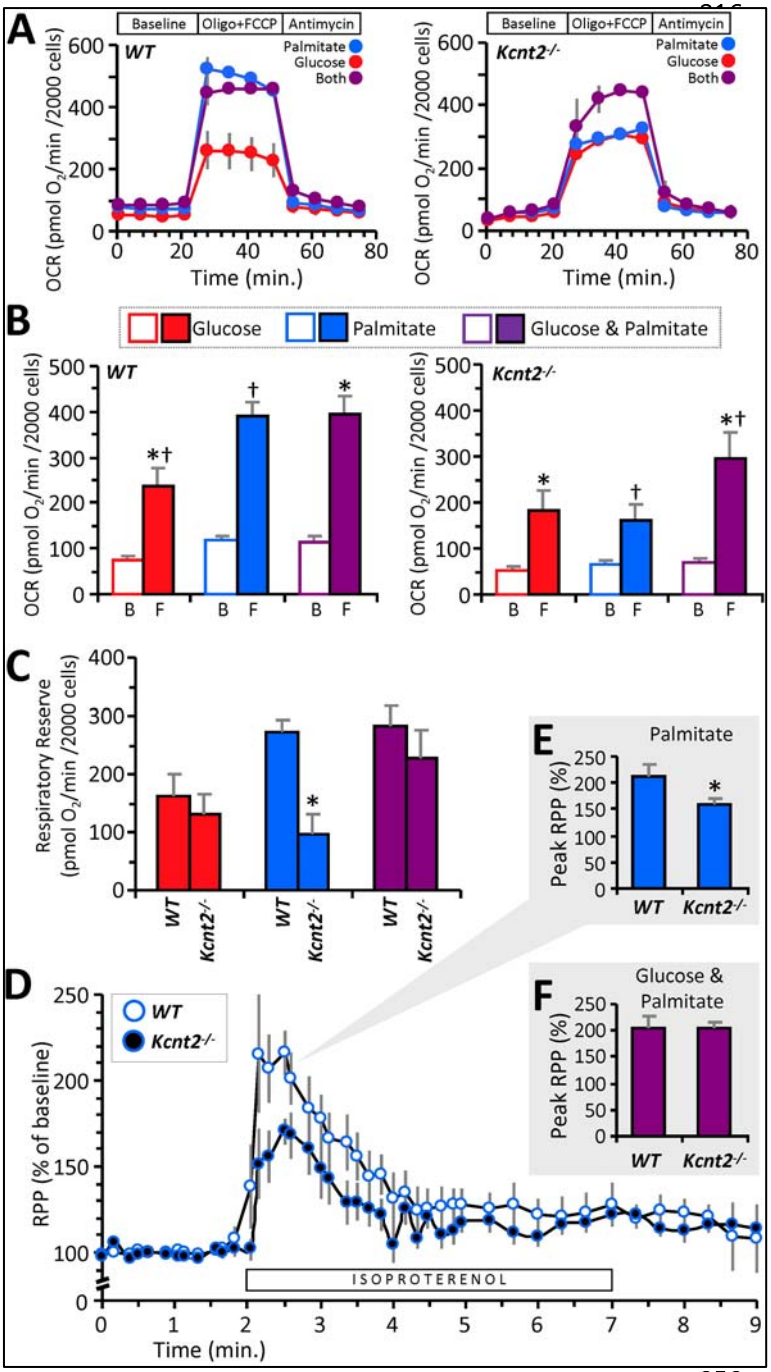

Figure 4: $K_{Na}1.2$ Impacts Cardiac Metabolic Substrate Choice under Stress. **(A)** Representative Seahorse XF oxygen consumption rate (OCR) traces of isolated WT or *Kcnt2*$^{-/-}$ cardiomyocytes, incubated in the presence of different metabolic substrates: glucose (red), palmitate (blue), glucose + palmitate (purple). Data from a single XF plate are shown (means ± SD of 12 wells per substrate or genotype). Timeline above traces shows OCR was measured at baseline, then with addition of the ATP synthase inhibitor oligomycin (1 µg/ml) plus the mitochondrial uncoupler FCCP (500 nM), and finally with the mitochondrial complex III inhibitor antimycin A (5 µM). **(B)** Group OCR averages of baseline (B) and FCCP-uncoupled (F) cardiomyocytes under substrate conditions as defined above. Statistics were measured using 2-way ANOVA with Bonferroni correction and post-hoc *t*-test. Data are means ± SEM, for N=4 (*Kcnt2*$^{-/-}$) or 5 (WT) independent cardiomyocyte preparations. Bars with the same symbol are significantly different from each other ($p<0.05$). **(C)** Respiratory reserve (RR) capacity calculated from the data in panel B (i.e., uncoupled minus baseline OCR). Means ± SEM, N=4-5, *$p<0.05$ between genotypes. Color key for panels B/C is shown above panel B. **(D)** Cardiac function data (heart rate x pressure product, RPP) for isolated perfused hearts from WT or *Kcnt2*$^{-/-}$ mice, perfused with Krebs-Henseleit (KH) buffer containing palmitate as the sole metabolic substrate. Bar below the trace indicates duration of 100 nM isoproterenol infusion. Graph shows RPP as a % of the average baseline value for 1 min before isoproterenol infusion. **(E)** Comparison of the peak response to isoproterenol under this substrate condition (palmitate only, blue). **(F)** shows peak response to isoproterenol from a separate series of perfusions in which the KH buffer contained both palmitate and glucose as substrates (purple). Data in E/F are means ± SEM, N=7, *$p<0.05$ between genotypes.

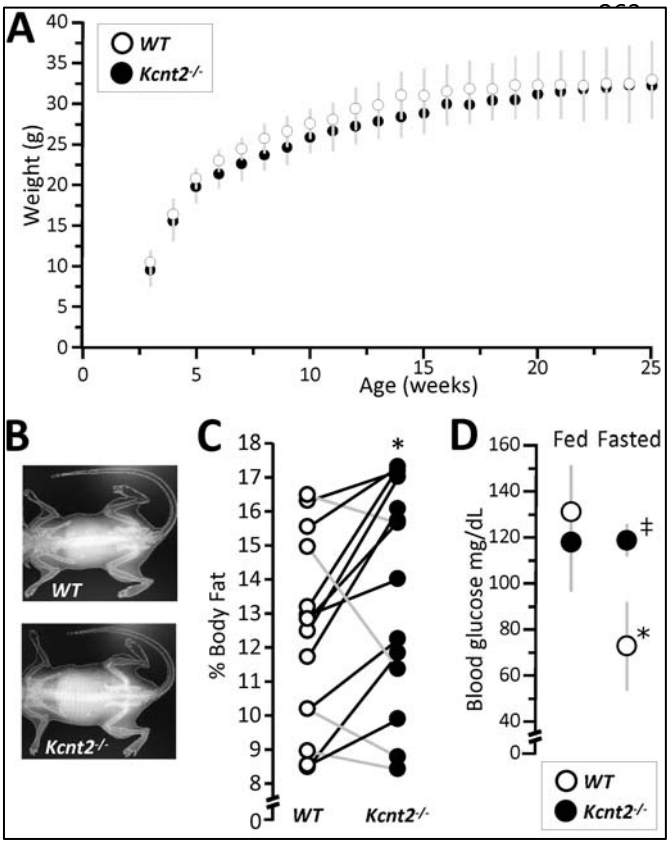

Figure 5: Loss of $K_{Na}1.2$ Impacts Whole Body Metabolic Phenotype. (A) Body weights of WT and *Kcnt2*$^{-/-}$ mice from weaning (3 weeks) to 25 weeks of age. Data are means ± SD, N=12. **(B)** Representative DEXA images from WT and *Kcnt2*$^{-/-}$ mice. **(C)** Percent body fat measured by DEXA scan of WT (white) and *Kcnt2*$^{-/-}$ (black) littermates (pair are indicated as data points connected by lines), N=14. *p<0.05 between genotypes by paired *t*-test. **(D)** Blood glucose levels measured in WT and *Kcnt2*$^{-/-}$ mice at baseline (5 PM, Fed) and following a 15 hr fast (8 AM, Fasted). Data are means ± SD, N=3. *p<0.05 between fed and fasted state within a genotype. ‡p<0.05 between genotypes at the same time point.

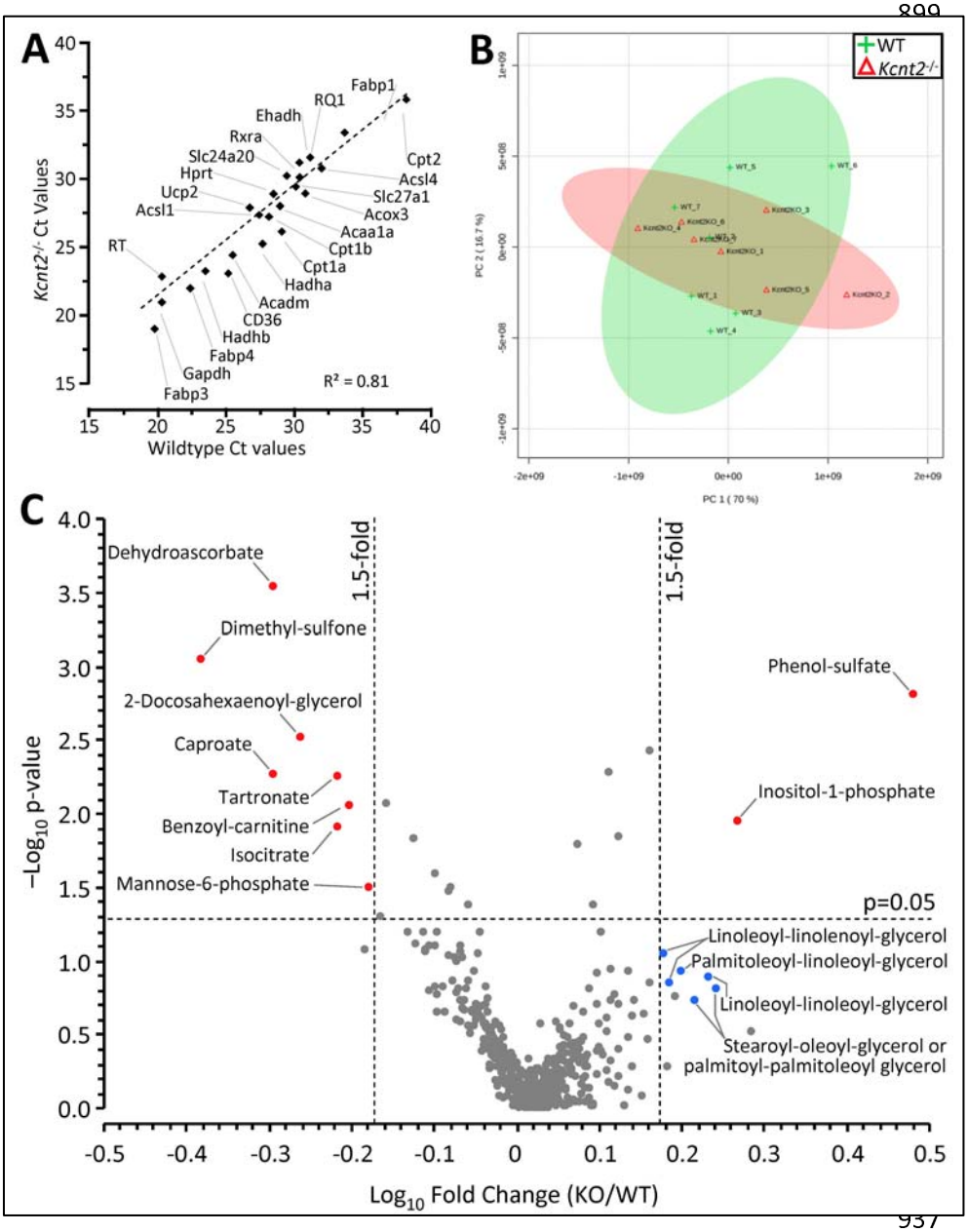

Figure 6: *Kcnt2*$^{-/-}$ Cardiac Expression Profiling and Metabolomics. (A) qPCR Ct values for 27 metabolically important genes (see Table S1), in WT and *Kcnt2*$^{-/-}$ hearts. N=3 independent RNA preparations per genotype. Data are means, errors are omitted for clarity. **(B)** WT and *Kcnt2*$^{-/-}$ hearts were perfused in rich-substrate KH buffer and freeze-clamped for metabolomic analysis by LC-MS/MS. Graph shows principle component analysis of 501 cardiac metabolites. The first and second principal components contributed 86.7% of the overall metabolic character. Shaded ovals overlaying the graph indicate 95% confidence intervals for WT (green) and *Kcnt2*$^{-/-}$ (pink) samples. **(C)** Volcano plot of the metabolic profile of *Kcnt2*$^{-/-}$ vs. WT hearts. Axes show -Log_{10}(p-value) vs. Log_{10}(fold change). Dashed lines show a p=0.05 cut off (y axis) and 1.5-fold change cut offs (x-axis). Each point represents a single metabolite, and data for each point are means from N=7 hearts. Errors are omitted for clarity. Metabolites passing fold-change and p-value criteria are highlighted red. Additional metabolites discussed in the text are highlighted blue.

Supplemental Online Information for

A Mitochondrial $K_{Na}1.2$ Channel Regulates Cardiac Energetics and Fat Metabolism

		Primary antibody			Secondary Antibody			Molecular Weight
Antibody	Manufacturer	Dilution	Blocking	Reactivity	Dilution	Blocking	reactivity	(kDa)
ACC	Elabscience ENT0075	1:1,000	5% Milk TBST	Rabbit	1:2,000	5% Milk TBST	goat anti rabbit	265
AMPK	Cell Signaling 23A3	1:1,000	5% BSA TBST	Rabbit	1:2,000	5% Milk TBST	goat anti rabbit	62
CypD		1:1,000	5% Milk TBST	Mouse	1:2,000	5% Milk TBST	goat anti mouse	18
EFTA	Abgent AP20630c	1:1,000	5% Milk TBST	Rabbit	1:2,000	5% Milk TBST	goat anti rabbit	35
GLUT4	Ameritech Biomed ATB-T1930	1:1,000	5% Milk TBST	Rabbit	1:2,000	5% Milk TBST	goat anti rabbit	50
ICDH	Abcam ab172964	1:10,000	5% Milk TBST	Rabbit	1:2,000	5% Milk TBST	goat anti rabbit	47
pACC (pSer80)	Elabscience ENP0595	1:1,000	5% Milk TBST	Rabbit	1:2,000	5% Milk TBST	goat anti rabbit	265
pAMPK (pThr127)	Cell Signaling 40H9	1:1,000	5% BSA TBST	Rabbit	1:2,000	5% Milk TBST	goat anti rabbit	62
PGC1a	Abcam Ab191838	1:1,000	5% Milk TBST	Rabbit	1:2,000	5% Milk TBST	goat anti rabbit	90
PMNKA	Abcam 7671	1:200	5% Milk TBST	Mouse	1:2,000	5% Milk TBST	goat anti mouse	112
PPARa	Boster Immuno PA1412	1:1,000	5% BSA TBST	Rabbit	1:2,000	5% Milk TBST	goat anti rabbit	55
PPARg	Abcam C26H12	1:100	5% BSA TBST	Rabbit	1:2,000	5% Milk TBST	goat anti rabbit	58
SDHA	Abcam14715	1:10,000	5% Milk TBST	Mouse	1:2,000	5% Milk TBST	goat anti mouse	70
SERCA	Abcam 2861	1:1,000	5% Milk TBST	Mouse	1:2,000	5% Milk TBST	goat anti mouse	70
VDAC	Millipore PC548	1:1,000	5% Milk TBST	Rabbit	1:2,000	5% Milk TBST	goat anti rabbit	31

Table S1. Antibodies used in this study. Antibody name, company, incubation conditions, secondary reactivity, and expected molecular weights for all antibodies reported (Figures 1B and S2).

Gene Name	Gene Symbol
Acetyl-Coenzyme A acyltransferase 1A	Acaa1a
Carnitine palmitoyltransferase 1a, liver	Cpt1a
Hydroxyacyl-Coenzyme A dehydrogenase/3-ketoacyl-Coenzyme A thiolase/enoyl-Coenzyme A hydratase (trifunctional protein), alpha subunit	Hadha
Acyl-Coenzyme A dehydrogenase, medium chain	Acadm
Carnitine palmitoyltransferase 1b, muscle	Cpt1b
Hydroxyacyl-Coenzyme A dehydrogenase/3-ketoacyl-Coenzyme A thiolase/enoyl-Coenzyme A hydratase (trifunctional protein), beta subunit	Hadhb
Glyceraldehyde-3-phosphate dehydrogenase	Gapdh
Acyl-Coenzyme A oxidase 3, pristanoyl	Acox3
Carnitine palmitoyltransferase 2	Cpt2
Hypoxanthine guanine phosphoribosyl transferase	Hprt
Acyl-CoA synthetase long-chain family member 1	Acsl1
Enoyl-Coenzyme A, hydratase/3-hydroxyacyl Coenzyme A dehydrogenase	Ehhadh
Retinoid X receptor alpha	Rxra
PrimePCR DNA Contamination Control Assay	gDNA
Fatty acid binding protein 1, liver	Fabp1
Solute carrier family 25 (mitochondrial carnitine/acylcarnitine translocase), member 20	Slc25a20
PrimePCR Positive Control Assay	PCR
Acyl-CoA synthetase long-chain family member 4	Acsl4
Solute carrier family 27 (fatty acid transporter), member 1	Slc27a1
PrimePCR RNA Quality Assay	RQ1
Fatty acid binding protein 3, muscle and heart	Fabp3
CD36 antigen	Cd36
Fatty acid binding protein 4, adipocyte	Fabp4
Uncoupling protein 2 (mitochondrial, proton carrier)	Ucp2
PrimePCR Reverse Transcription Control Assay	RT

Table S2. Gene names and symbols for genes targeted by BioRad PrimePCR qPCR assay kit (Figure 6A)

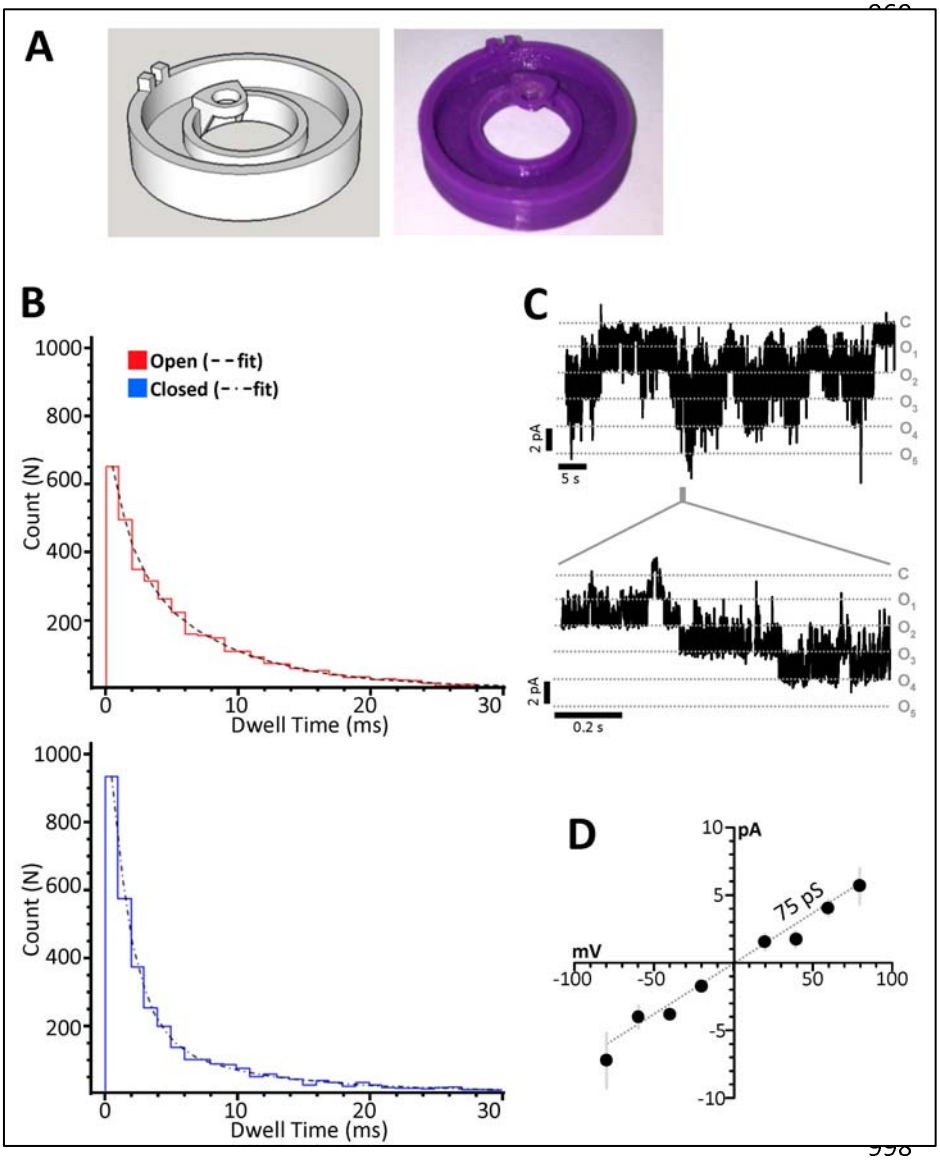

Figure S1: (A) Custom 3D printed micro chamber for patch-clamp of mitoplasts with computer model (left) and final product (right). Stereolithography file is deposited at: https://3dprint.nih.gov/discover/3dpx-008253. **(B)** Frequency of open (red) and closed (blue) dwell times plotted against their duration (from Figure 2E). **(C)** Expanded traces from recordings of patches containing five mitochondrial $K_{Na}1.2$ channels (holding potential -20mV) and a time expanded trace for the region highlighted by the gray bar in the trace above. Graydotted lines represent closed ("C") and multiple open (O_1, O_2, O_3, etc.) states. **(D)** Current Voltage relationship of all six mito-$K_{Na}1.2$ channels showing average current at each holding potential. The decreased slope conductance (compared to Figure 2B showing peak unitary conductance) indicates that subconductances averaging 75 pS dominate the average current during the recordings.

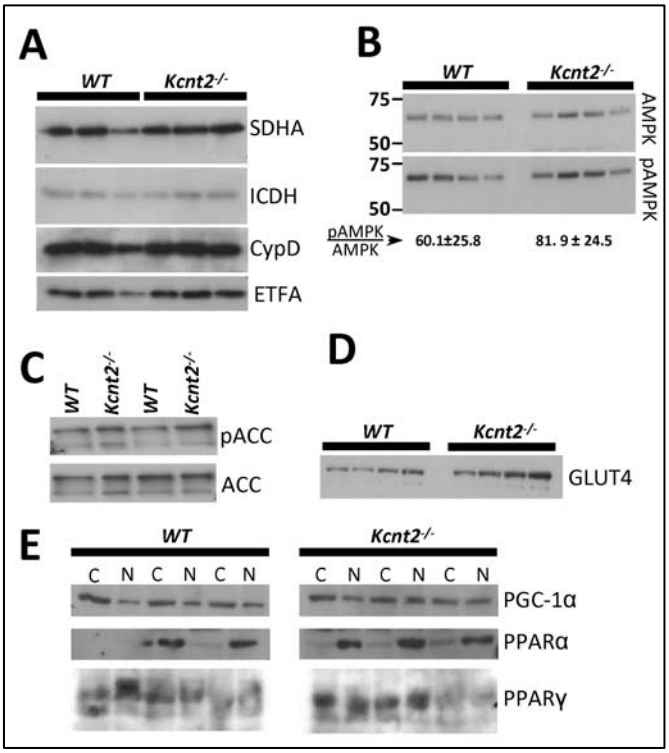

1030

1031 **Figure S2:** Western blots from WT and *Kcnt2*$^{-/-}$ homogenates showing levels of: **(A)**
1032 Mitochondrial proteins (SDHA, ICDH, CypD and EFTA). **(B)** AMPK and phospho-AMPK. Values
1033 below the blot show pAMPK/AMPK ratio (densitometry, normalized to protein loading). Means
1034 ± SD from the 4 independent lanes. **(C)** ACC and phospho-ACC. **(D)** GLUT4. **(E)** PGC1α, PPARα,
1035 and PPARγ. In this panel, C denotes cytosol, N denotes nuclear fraction. See Table S1 for
1036 antibody descriptions.
1037

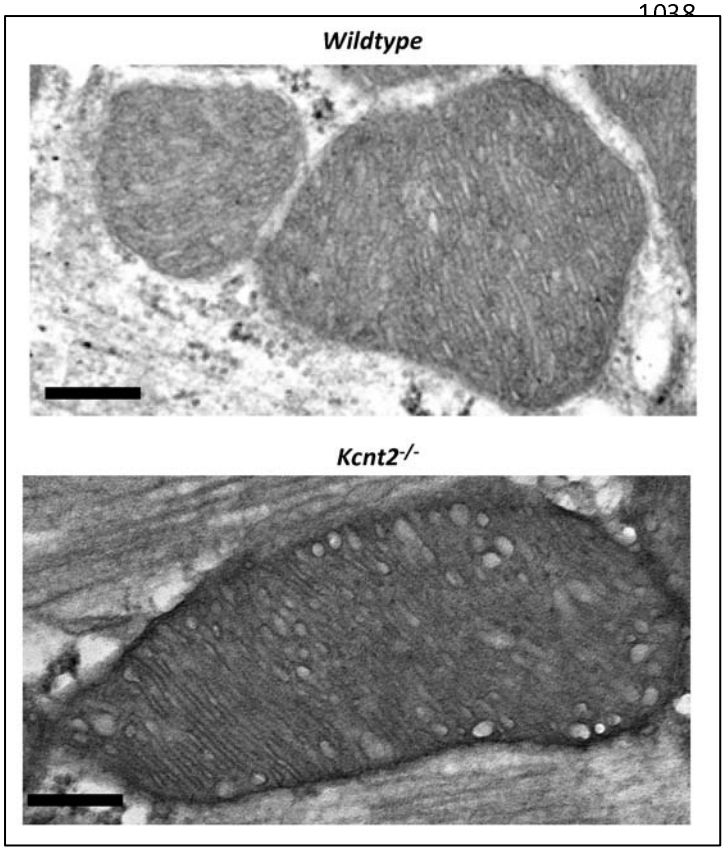

Figure S3: Increased magnification of heart mitochondria from WT and *Kcnt2*$^{-/-}$ mice with mitochondrial ultrastructure (i.e. cristae folds, outer and inner membrane contacts) visible. Scale bar 200 nm.

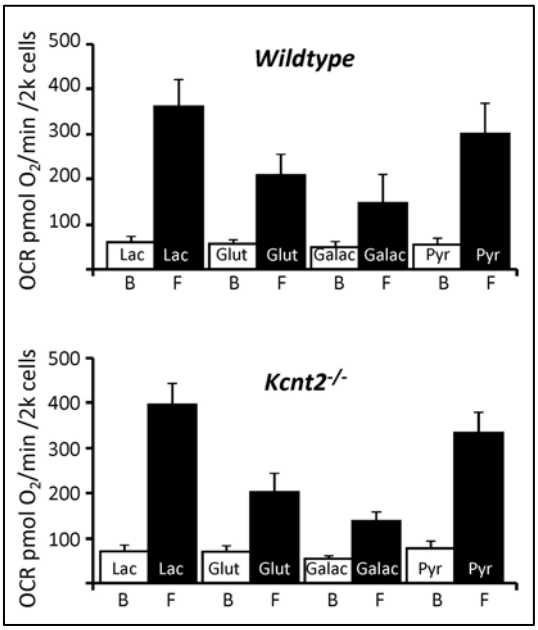

1082

1083 **Figure S4**: Oxygen consumption rates (OCR) of WT and *Kcnt2*$^{-/-}$ cardiomyocytes metabolizing
1084 different substrates: lactate, glutamate, galactose, or pyruvate. White bars = baseline (B), black
1085 bars = FCCP uncoupled (F). Data are companion to Figure 4B and are presented in the same
1086 manner (i.e. means ± SEM from 4-5 independent cardiomyocyte preparations).
1087
1088

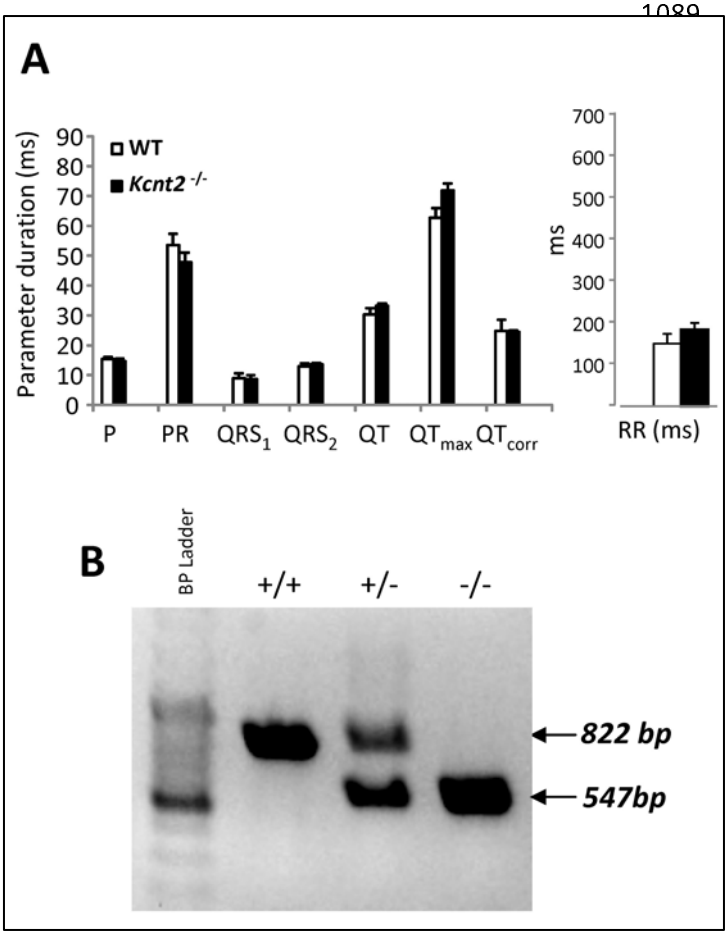

Figure S5: (A) EKG parameters obtained *in-vivo* from WT and *Kcnt2*$^{-/-}$ mice. P = p-wave duration. PR = interval between P and R waves. QRS1 & QRS2 – diameter of QRS complex (different calculation algorithms). QT = interval between Q and peak of T wave. QT_{max} = interval between Q and end of T wave. QT_{corr} = QT interval corrected for heart rate. RR = distance between R waves of each beat (i.e. 1/HR). **(B)** PCR analysis of tail clip genotyping of WT, heterozygous, and *Kcnt2*$^{-/-}$, mice. 822 bp amplicon expected for WT allele and 547 bp expected for knockout allele.